Photochemical Modeling of Two 1984 SCCCAMP Ozone Episodes

T. W. TESCHE

Alpine Geophysics, Crested Butte, Colorado

DENNIS E. MCNALLY

Numerical Solutions, Golden, Colorado

(Manuscript received 15 January 1990, in final form 31 October 1990)

ABSTRACT

Data collected during the 1984 SCCCAMP Exploratory Study were used to develop two multiple-day ozone modeling episodes for the Urban Airshed Model (UAM). An operational model performance evaluation was performed for the 5–7 and 16–17 September 1984 episodes. Peak 1-h average ozone concentrations were reproduced on the five simulation days with accuracies (paired in time and space) ranging from 0% to −30%. The mean bias in hourly averaged ozone concentrations ranged from −6% to +11%, and the mean gross errors varied between 23% and 38%. UAM performance for ozone concentrations with the two September episodes is comparable with other recent photochemical model evaluations. Lack of sufficient measurements for model performance testing of other important photochemical species (e.g., NO, NO_2, volatile organic compounds) and for carrying out compensatory error analysis and related diagnostic and mechanistic investigations precluded a more rigorous scientific evaluation of UAM performance with the 1984 SCCCAMP database.

1. Introduction

Decision makers face several complex planning issues related to urban- and regional-scale ozone air pollution. For example, will nitrogen oxides (NO_x) control accelerate or impede progress toward ozone attainment? Can photochemical models be relied upon to estimate the future impacts of emission control programs implemented now? Can models simulate adequately the effects of individual sources or source categories of air pollution? Can effective reactive organic gas (ROG) and NO_x emission reduction strategies be derived from models, weighing the desires for ozone attainment, reduction of public health impacts, and other policy goals? Can models attribute specific portions of a local ozone exceedence to near versus upwind source regions?

During the 1980s, photochemical grid models emerged as practical regulatory tools for estimating ozone air pollution impacts in urban and regional settings. Eulerian models such as the Urban Airshed Model (UAM) provide a quantitative link between source emissions and receptor concentrations at a level of detail unavailable through simpler modeling methods. Given high-resolution emissions and aerometric databases, photochemical grid models are generally able to reproduce hourly-averaged ozone concentrations, paired in space, to within 30%–35%. The maximum 1-h value during a 2–3 day episode can often be simulated to within 5%–10% (Tesche 1988). Given the enormous economic costs associated with ozone control programs in the United States, the use of photochemical grid models represents a technically viable, cost-effective method for air quality planning, provided adequate databases are available for model performance testing.

This paper reports the development of two multiple-day ozone modeling episodes and subsequent model performance evaluation activities carried out in support of the 1989 Air Quality Attainment Plan (AQAP) for Santa Barbara County and EPA's Federal Implementation Plan (FIP) for Ventura County. Both counties are portions of the south-central coast air basin (SCCAB), shown in Fig. 1. The two episodes were selected from the 1984 South-Central Coast Cooperative Aerometric Monitoring Program (SCCCAMP), described in detail by Dabberdt and Viezee (1987). Databases for 5–7 September 1984 and 16–17 September 1984 were constructed for the UAM to facilitate an operational performance evaluation, consisting of a series of graphical and statistical comparisons and extensive sensitivity analyses. Details of the photochemical modeling work are contained in the two project reports (Tesche et al. 1988a; Tesche and McNally 1989).

Several photochemical modeling studies have been carried out in the Santa Barbara–Ventura region. The first was the Joint Interagency Modeling Study (JIMS)

Corresponding author address: Dr. Thomas Tesche, Alpine Geophysics, P.O. Box 2059, Crested Butte, Co 81224.

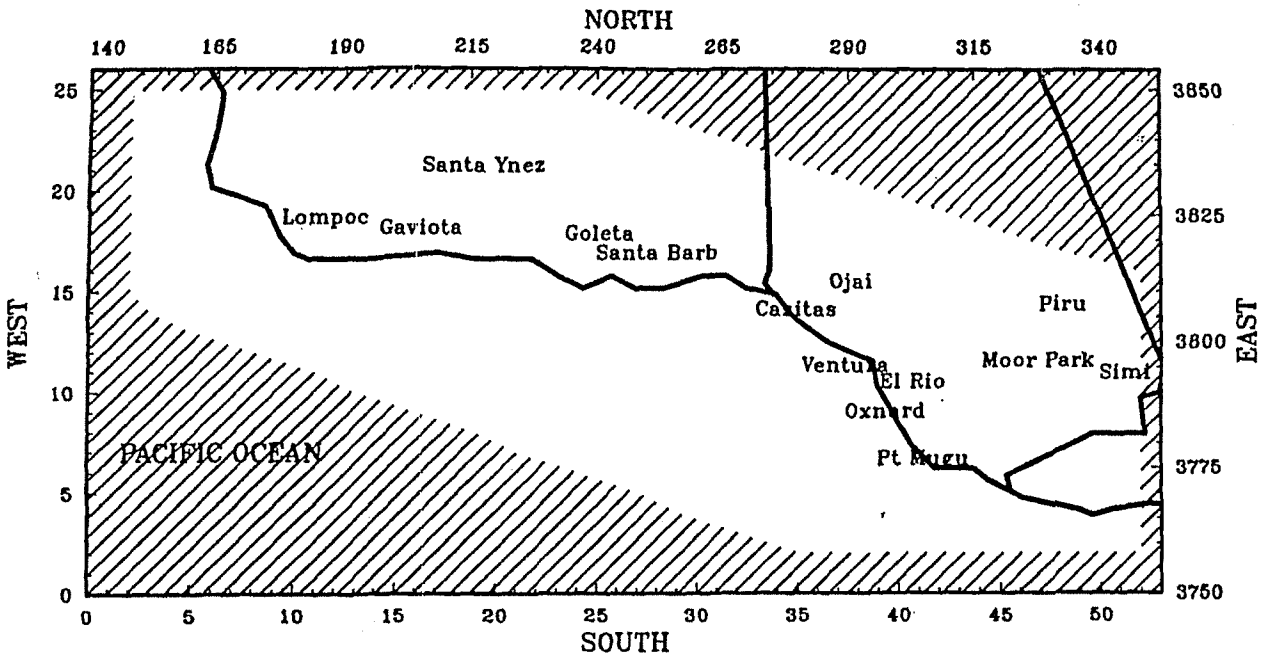

FIG. 1. The south-central coast air basin modeling and analysis region.

(Haney et al. 1986) in which the UAM was evaluated for three, 2-day episodes from the 1980 Santa Barbara Channel Oxidant Study. The California State Lands Commission sponsored a model evaluation effort with the 27–28 September 1984 SCCCAMP ozone episode (SLC 1986), and the California Air Resources Board (ARB) developed modeling databases for three ozone episodes from the 1895 SCCCAMP field program (Wagner 1989). Each of these studies included model performance testing and limited sensitivity analysis.

Section 2 summarizes the aerometric features of the two 1984 SCCCAMP ozone episodes used in this study. The photochemical and meteorological models selected and the input preparation procedures employed are described in sections 3 and 4, respectively. In section 5, we suggest an approach to rigorous model performance evaluation that should accompany every photochemical modeling study where sufficient data are available. Section 6 summarizes the operational evaluation results for both episodes. The principal limitations of the present evaluation, related primarily to database constraints, are discussed in section 7. Our conclusions are presented in section 8.

2. The 1984 SCCCAMP Exploratory Field Study

The 1984 SCCCAMP Exploratory Field Study consisted of continuous aerometric monitoring and intensive measurements specifically designed to test sampling techniques and to provide the basis for more refined experiments the following year (Dabberdt 1984). These experiments included enhanced measurements of surface and upper-level winds, NO_x and ROG speciation, aircraft soundings, and chemical species sampling. Following the field work, SCCCAMP sponsored an analysis of the 1984 data (Tesche et al. 1985) to strengthen the design of the 1985 measurement program and to assess the suitability of the 1984 database for photochemical modeling. The first activity aided in formulating the 1985 SCCCAMP monitoring program study design and experimental protocol (Reynolds et al. 1985; Dabberdt and Viezee 1987), while the second activity led to a conceptual model of the meteorology and air quality during the sampling period.

The September 1984 data indicated that surface winds in the SCCAB follow a diurnal pattern composed of two major regimes: an afternoon–evening sea-breeze flow; and a nighttime–morning drainage flow. The sea-breeze influence is strongest over the Oxnard plain, which is directly exposed to the westerly wind flow across the Santa Barbara Channel. Some of this westerly flow is deflected south of the Santa Monica Mountains toward Los Angeles. Although onshore winds influence the flow regimes in mountain areas, an upper-level southeasterly flow was dominant during this study period above 750 m MSL. Drainage winds were an order of magnitude weaker than their onshore counterparts, and were most pronounced in channeling situations, such as in the Santa Clara River valley. Lack of data from the Santa Barbara Channel area limited characterization of the nocturnal counterclockwise eddy over the northern half of the channel. Similarly, data are needed in the vicinity of Gaviota Pass to reveal more clearly the formation of eddies by winds rounding Point

Conception. Still, there is evidence in the 1984 data of a nocturnal counterclockwise eddy over the northern portion of the Santa Monica Bay.

Upper-level air flow at six stations during September 1984 is dominated by easterly to southeasterly winds above 750–1000 m. Below 500–750 m, winds at all stations are affected by diurnal offshore–onshore flows. Strong onshore flows appear to push the lower level of the southeasterlies upward, creating a sharply defined shear zone within the boundary layer.

The timing of sea-breeze episodes varies daily but, typically, the sea breeze peaks over the Oxnard plain at about 1500 PST. This timing does not appear to be a function of distance from the coast. During the 5–7 September episode, winds were generally light and there was considerable airmass stagnation over the Santa Barbara Channel area and coastal regions. The 16–17 September ozone episode was preceded by two days of strong offshore (easterly-to-southeasterly) winds aloft; sea-breeze episodes were weak. A subsidence inversion kept vertical mixing to a minimum. On the afternoon of the 17th, the sea breeze strengthened slightly and the inversion weakened, allowing previously stagnant air to move inland and a limited amount of mixing with the upper air to occur.

Hourly averaged ozone measurements were performed during September 1984 at 16 monitoring stations. For the two episodes modeled here, the six highest stations and their respective ozone maxima are listed in Table 1. Both episodes exhibit widespread ozone levels above the federal 1-h standard (12 pphm). The 5–7 September episode not only has the higher ozone maximum (18 pphm at Casitas on the 7th), but the overall ozone concentrations for this period are greater than for 16–17 September. Both episodes coincide with peaks in the morning 850-mb temperature, a strong indicator of high ozone formation potential in southern California. During the 5–7 September period, the region of maximum afternoon ozone was shifted westward from the eastern basin on the 6th (near Simi) to a midbasin location (Casitas) on the 7th. High ozone levels are reported in Santa Barbara County on this day. A similar westerly shift does not appear on the 16–17 September.

3. Description of the models

The models used in this study included the Urban Airshed Model (UAM-II) (Ames et al. 1985), an objective analysis wind model (Goodin et al. 1980), and a modified version of the Steyn–Oke mixing-height model (Steyn and Oke 1982). Brief descriptions of each model are given here since full details are reported elsewhere.

a. The Urban Airshed Model

The UAM is an Eulerian photochemical model that simulates the emission, transport, dispersion, chemical transformation, and removal of inert and chemically reactive species in the atmospheric boundary layer (Ames et al. 1985; Morris et al. 1990). The UAM is EPA's current guideline model for refined analysis of urban ozone air pollution (EPA, 1986). Time evolution of chemically reactive pollutants are simulated through numerical solution of the species mass conservation equation, given by

$$\frac{\partial \tilde{C}_i}{\partial t} + \frac{\partial}{\partial x}(u\tilde{C}_i) + \frac{\partial}{\partial y}(v\tilde{C}_i) + \frac{\partial}{\partial z}(w\tilde{C}_i) = \frac{\partial}{\partial x} K_H \frac{\partial \tilde{C}_i}{\partial x} + \frac{\partial}{\partial y} K_H \frac{\partial \tilde{C}_i}{\partial y} + \frac{\partial}{\partial z} K_V \frac{\partial \tilde{C}_i}{\partial z} + R_i(\tilde{C}_1, \cdots, \tilde{C}_N, t) + S_i(x, y, z, t) + R_{ni}(x, y, z, t) \quad (1)$$

where the symbol ~ represents a spatial averaging operation; C_i = the estimated value of the instantaneous concentration of pollutant i; u, v, and w = the mean wind velocity components; K_h and K_V = the horizonal and vertical eddy diffusivity components; S_i = the rate of emission of pollutant i from surface and elevated sources; R_i = the contribution of the mean concentration to the net reaction rate of pollutant i; and R_{ni} = the dry deposition rate of species i. The governing equations are coupled, nonlinear, multidimensional, and time dependent. They are ensemble-averaged and integrated using an explicit finite-difference solution

TABLE 1. Peak ozone concentrations (pphm) during the two 1984 SCCCAMP episodes.

5 September		6 September		7 September		16 September		17 September	
Maxima	Station	Maxima	Station	Maxima	Station	Maxima	Station	Maxima	Station
10	Casitas Pass	17	Simi	18	Casitas Pass	11	Simi	14	Casitas Pass
9	Simi	16	Piru	15	Goleta	9	Thousand Oaks	13	Simi
8	Gaviota	16	Thousand Oaks	15	Santa Barbara	6	Piru	12	Thousand Oaks
7	Thousand Oaks	13	Ojai	13	Simi	8	Ojai	12	Santa Barbara
7	Ojai	13	Casitas Pass	13	Ojai	8	Casitas Pass	12	Ojai
		10	El Capitan	11	El Capitan, Thousand Oaks	7	Ventura	11	Goleta

technique. Advective and diffusive transport are treated sequentially using the method of fractional steps. The Smolarkiewicz (1983) method is employed to solve the advective part of the problem. The UAM is based on a terrain-following coordinate system.

For more than a decade, EPA distributed the UAM with the carbon bond II (CBM-II) kinetic mechanism (Whitten et al. 1980). This version simulates the chemical reactions of NO, NO_2, ozone, HNO_2, H_2O_2, paraffins, olefins, aromatics, aldehydes, carbonyls, PAN, SO_2, CO, sulfate aerosol, and total aerosol mass concentration. EPA released an updated version of the UAM with carbon bond IV chemistry (UAM-IV) (Gery et al. 1988) in September 1990. Details of the UAM-IV are given in Morris et al. (1990).

The UAM requires meteorological inputs that include a three-dimensional wind field, the vertical thermal structure, and estimates of the mixing height above each grid cell within the modeling domain as a function of time. Surface temperature fields and solar radiation intensity data are also needed for each simulation hour. Wind field inputs to the UAM historically have been developed through the use of simple interpolation models. Based on surface and upper-air meteorological data, these interpolation, extrapolation, and divergence-reduction routines are employed to develop three-dimensional flow fields. More recently, diagnostic and prognostic wind field models have become preferred means of constructing the transport fields (Tesche 1991).

An area and elevated source-emissions description is needed giving the temporal and spatial distribution of the pollutants emitted from all sources within the modeling region. These emission estimates have historically been developed by state and local regulatory agencies and their computation involves the use of a wide variety of calculational procedures. Dry removal processes are treated as surface boundary conditions.

The UAM estimates ozone, precursor species, and product species (e.g., nitric acid and PAN) for each hour of the simulation in all grid cells in the computational domain. Typically, the model is operated for episodes of 2–3 days duration so that the effects of uncertainties in initial conditions are minimized by the second or third simulation day. Model output is displayed in time series plots for various monitoring stations, affording comparisons between hourly average model estimates and observations. Ground-level-concentration isopleths may be plotted for various hours of each simulation day to reveal the spatial distribution of ozone concentrations and other species of interest.

b. The meteorological model

Transport fields were developed in this study using the interpolation model of Goodin et al. (1980). This wind model is a three-dimensional, objective analysis scheme that invokes mass consistency constraints. The model uses a two-step procedure. First, ground-level wind measurements are interpolated to give a surface flow field. Then, the upper-level winds (i.e., above the surface layer) are objectively analyzed to render the resultant three-dimensional flow field mass conserving. This is achieved by strongly constraining the vertical velocity. In most cases, an adjustment is made to the vertical velocity field so that the net mass transport through the model top is zero. The model uses terrain-following coordinates and a variable vertical grid mesh. Vertical velocities are determined from successive iterations of the mass conservation equation, reducing field divergence to a prescribed level. The method is computationally efficient and has been widely applied as a meteorological preprocessor in photochemical modeling studies. However, its performance is difficult to assess since it uses all available, valid wind information to construct the flow fields.

c. The mixing-height model

Several modeling procedures are available for estimating mixing heights in coastal-complex terrain. The model developed by Steyn and Oke (1982) was selected for daytime mixing-height estimation because it is formulated for coastal convective boundary layers and it directly utilizes the surface and upper-air meteorological measurements collected during SCCCAMP. The Steyn–Oke model is an extension of the Tennekes (1973) zero-order jump model, a generalized thermodynamic treatment of convective boundary-layer development. Steyn and Oke included the effects of advection and inversion subsidence, two physical processes of significance in coastal settings. The model consists of a coupled, nonlinear system of ordinary differential equations that are solved numerically given prescribed initial and boundary conditions. The Steyn–Oke model was refined in this study to include algorithms for computing the turbulent sensible heat flux as a function of surface meteorological variables and distance from the irregular SCCAB coastline.

4. Preparation of Urban Airshed Model inputs

The UAM modeling region consists of a 53 × 26 grid domain with 4-km horizontal resolution. Use of finer grid resolution, potentially helpful in resolving transport processes occurring near the coastline and mountain slopes, was impractical since the emissions grid, previously developed by state and local agencies, was fixed at 4 km. The vertical grid structure was based upon analysis of the windfields, mixing heights, aircraft measurements, and emissions source heights in the basin. The vertical grid definition consists of four vertical levels with two above the inversion and two below. A modeling domain height was set at 1000 m.

a. 1984 SCCCAMP database

The 1984 SCCCAMP Exploratory Field Study provided a database that was significantly richer than that

TABLE 2. Total precursor emissions (kg day^{-1}) for 1984 in the south-central coast air basin.

	6 September	7 September	16 September	17 September
Point sources:				
NO	20 725	22 169	19 489	18 908
NO_2	1671	1788	1572	1525
ROG	1651	2188	1614	1460
Area sources:				
NO	51 313	51 370	44 272	51 301
NO_2	4138	4143	3570	4137
ROG	113 434	112 579	94 548	112 462

afforded by the routine monitoring activities in the basin. Surface wind data, collected hourly, were available from 17 onshore sites and from 3 offshore oil production platforms. Upper-level wind monitoring was performed at five sites, supplementing the routine data collection at Point Mugu and Vandenberg Air Force Base. Twelve surface temperature stations were in operation and vertical temperature profiles were available twice daily at Vandenberg and three times a day at Point Mugu. In addition, during the 16–17 September episode, 25 vertical aircraft soundings were performed over land and water for upper air characterization. During the period 10–22 September, a total of 15 aircraft flights were performed over strategic portions of the basin, documenting the vertical and horizontal extent of temperature, humidity, turbulence, NO_x, ozone, and *b*-scat fields. This intensive measurement set combined with the information from the routine surface aerometric database represented the available database with which UAM inputs for the September episodes were prepared.

b. The emissions estimates

The UAM requires emissions estimates for all relevant anthropogenic and natural sources in the modeling region. The emissions used in this study were resolved on a 4-km grid, temporally allocated (i.e., hourly emissions estimates), and disaggregated according to NO_x and reactive organic gas (ROG) chemical species. Emissions rates for all sources in the region were constructed from baseline estimates for total organic gas (TOG), NO_x, PM, SO_2, and CO.

The emissions estimation process was carried out by the California Air Resources Board and the two local air pollution control districts. It involved the following steps: (a) source identification; (b) source and process characterization; (c) source activity level determination; (d) emission factor estimation; (e) emission rate calculation; and (f) emission gridding, temporal splitting, and species allocation. Emissions estimates were distributed temporally and spatially, including in the vertical plane, consistent with the UAM grid mesh. Point sources were located with specific coordinates identifying their position in the grid region. Since the UAM uses stack data to compute plume rise for all point source emissions based on hourly meteorological conditions, this information was compiled as well. Area source emissions were allocated to grid cells using surrogate information such as population or industrial employment distributions for each source category. Operating schedules for typical point and area sources were used for resolving temporary emissions data to specific time periods. Day-specific emissions information, typically gathered for large point sources, was not compiled for 1984.

TABLE 3. Estimated maximum mixed-layer heights (m) at 12 monitoring stations for the September 1984 episodes.

Monitoring station	5 September	6 September	7 September	16 September	17 September
Point Mugu	152	200	253	179	152
Santa Ynez	401	425	469	608	357
Santa Barbara	271	226	286	384	246
Ojai	282	227	427	421	319
Piru	404	329	466	626	369
Simi	374	282	529	509	359
Moorpark	362	279	503	501	356
Thousand Oaks	335	238	488	482	353
Oxnard	187	200	448	259	213
Vandenberg	203	162	255	349	292
Lompoc	315	400	394	501	357
Santa Paula	363	283	439	514	377
Average	304	271	413	444	313

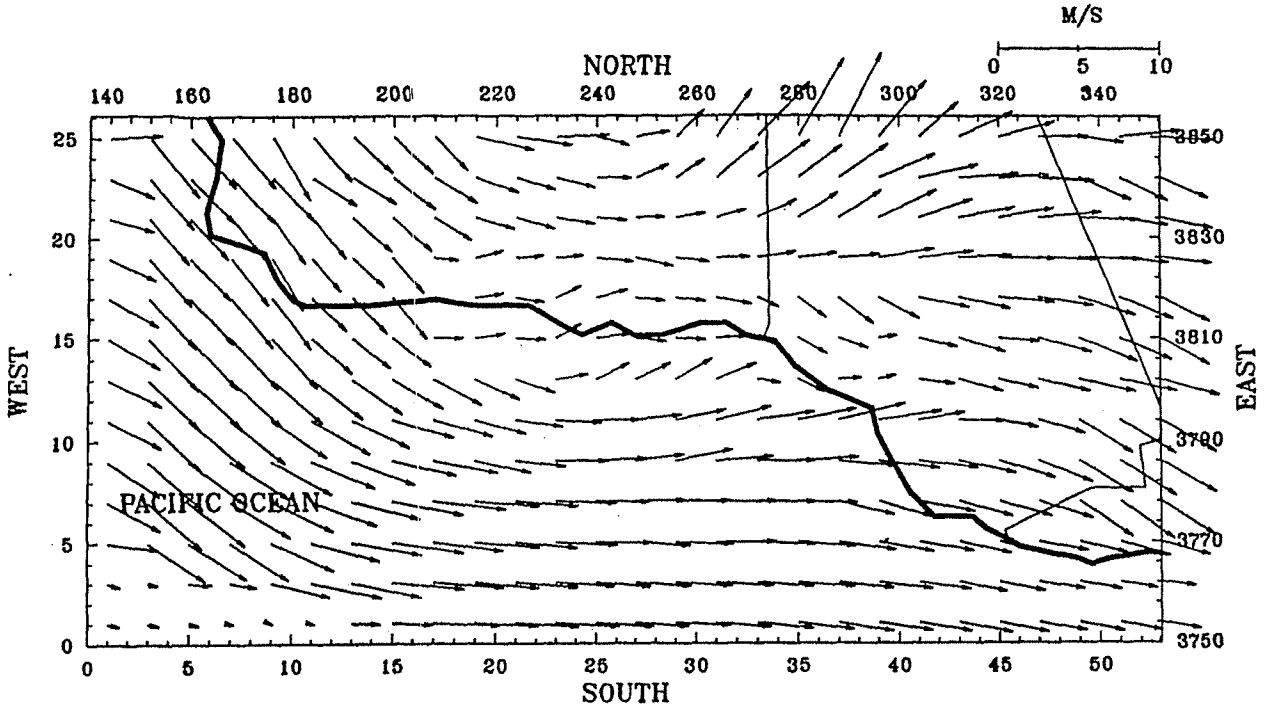

FIG. 2. Hourly surface flow field at 1600 PST 5 September 1984.

Table 2 gives emissions totals (kg day^{-1}) for NO, NO_2, and ROG for each simulation day for both point and area source files. (Emissions on the 5th were assumed to be identical to those on the 6th.) Total daily point source NO_x emissions vary slightly from the 4-day average, from −7% to +9%. For point source ROG emissions, the variation from day to day is larger on a percentage basis, from −16% to +27%. For the area sources, the variation in NO_x and ROG emissions is −11% to +4% and −13% to +5%, respectively.

c. *Scalar inputs*

The UAM requires a number of scalar quantities to calculate atmospheric stabilities, turbulent diffusivities, surface deposition rates, plume rise, and so on. Available meteorological observations were used with boundary-layer parameterization schemes (Holtslag and van Ulden 1983; van Ulden and Holtslag 1985; Wilczak and Phillips 1986) to calculate the surface turbulent heat flux, friction velocity, Monin–Obukhov length scale, turbulence intensity, convective velocity scale, and the temperature scale for turbulent heat transfer. These parameters were calculated hourly based on gridded terrain elevations, surface roughness, and vegetation factors, and estimates of local surface wind speed and direction, early morning temperature soundings, surface albedo, and soil moisture content.

d. *Mixing heights*

The UAM uses the mixing-height concept to divide the modeling domain into two regions that differ significantly in their turbulent structures. For convective and neutral boundary layers under a strong subsidence inversion, this division into two regions is generally adequate. For the nocturnal stable boundary layer, however, finer discritization of the vertical grid mesh is desirable, particularly under stable nighttime conditions. As a compromise, a vertical grid mesh of four levels, with two cells below the nominal daytime mixing height and two cells above, was used.

The 1984 SCCCAMP study did not provide sufficient data for quantitative evaluation of the mixing-height estimates for the two September episodes. One motivation for using the Steyn–Oke model was that it incorporates greater physical realism and utilizes more of the meteorological data than other readily available

TABLE 4. Nominal inflow boundary conditions for September 1984 simulations (except as noted in text).

Species	Concentration (ppm)
NO	0.001
NO_2	0.001
O_3	0.040
CO	0.200
ETH	0.0010
OLE	0.00057
PAR	0.0215
CARB	0.00073
ARO	0.0039
PAN	0.0005
BZA	0.00001

methods. As noted, the original model formulation was modified in this study to incorporate local topographic features of the SCCAB and to compute the turbulent sensible heat flux from routine NWS observations. The modified model was then exercised with hourly data to compute daytime convective mixing heights at 12 onshore locations in the basin. Table 3 lists the maximum daytime mixing heights derived in this manner. For nighttime periods when the Steyn–Oke model is not applicable (e.g., 2000–0600 PST), we assumed a constant mixed-layer height of 75 m over the entire modeling domain, consistent with previous UAM studies in the region.

e. *Wind fields*

The three-dimensional wind field is one of the most important inputs to the UAM. A preferred approach to wind-field construction, particularly in coastal settings, is the use of a prognostic meteorological model (Kessler and Douglas 1989; Stauffer and Seaman 1990; Tesche 1991). Resource constraints in this study precluded this approach so we used the simple interpolation model of Goodin et al. (1980). Thirty surface and six upper-air wind stations were used as inputs to the wind interpolation model. Initial results from the wind model using only the reported data gave surface flow fields that were inadequate for photochemical modeling, primarily because most of the observational data are either along the very narrow Santa Barbara County coastal margin, or distributed throughout the Oxnard plain and the inland coastal valleys. With the exception of a few offshore platform wind stations adjacent to the coast and the two buoys near Point Conception, there is very little wind information over the ocean. Moreover, wind data over elevated, complex terrain was absent in SCCCAMP 1984. These two regions, overwater and the mountains, represent large portions of the UAM computational domain.

Lack of wind data in key areas required that we supplement the observational data in regions where data were missing or in short supply. Key subareas were identified where the local flow patterns were found, through initial interpolation, to be inadequately characterized. Supplemental speed and direction values were developed for different portions of the day based on the original interpolated wind field, observed surface and upper-air winds, the conceptual model of the episode, and previous modeling experience in the SCCAB. The conceptual model of diurnal surface flow fields (Tesche et al. 1985) guided the assignment of these supplemental wind inputs. Figure 2 is an example of the estimated surface winds at 1600 PST on 5 September. Details of the hourly flow fields for each episode are contained in the project reports.

TABLE 5. Inflow boundary conditions along the southeastern portion of the modeling region.

Hour	5–7 September 1948				16–17 September 1984			
(PST)	NO	NO_2	O_3	RHC	NO	NO_2	O_3	RHC
0–1	0.001	0.001	0.04	0.100	0.001	0.001	0.04	0.100
1–2	0.031	0.033	0.00	0.761	0.007	0.025	0.00	0.388
2–3	0.031	0.034	0.00	0.781	0.010	0.027	0.00	0.450
3–4	0.025	0.035	0.00	0.782	0.009	0.029	0.00	0.500
4–5	0.017	0.032	0.00	0.729	0.008	0.030	0.00	0.538
5–6	0.011	0.026	0.01	0.637	0.013	0.029	0.00	0.554
6–7	0.010	0.036	0.04	0.689	0.013	0.032	0.02	0.588
7–8	0.010	0.036	0.04	0.689	0.008	0.034	0.05	0.607
8–9	0.003	0.022	0.09	0.533	0.004	0.024	0.10	0.559
9–10	0.001	0.006	0.11	0.308	0.001	0.008	0.12	0.387
10–11	0.001	0.002	0.10	0.206	0.001	0.003	0.09	0.238
11–12	0.001	0.002	0.09	0.172	0.001	0.003	0.05	0.156
20–21	0.001	0.005	0.05	0.174	0.001	0.006	0.04	0.176
21–22	0.001	0.007	0.04	0.200	0.001	0.009	0.04	0.200
22–23	0.001	0.012	0.04	0.233	0.001	0.009	0.04	0.200
23–24	0.001	0.012	0.04	0.233	0.001	0.009	0.04	0.200

TABLE 6. Hydrocarbon splits used to apportion VOC measurements into carbon bond II species groups.

Carbon bond II component	5–7 September Fraction (as carbon)	5–7 September Fraction	16–17 September Fraction (as carbon)	16–17 September Fraction
PAR	0.778	0.778	0.770	0.770
ARO	0.152	0.025	0.153	0.026
CARB	0.021	0.021	0.027	0.027
OLE	0.020	0.010	0.018	0.009
ETH	0.031	0.016	0.030	0.015

f. *Initial and boundary conditions*

Initial conditions for NO, NO_2, ozone, and ROG were derived from the interpolation and extrapolation of observed concentration values at the beginning of the two simulation periods (0200 PST, 5 and 16 September). Initial conditions were based on the vertical grid structure, boundary concentrations aloft, and ambient pollutant measurements. The available aircraft measurements on the 16th and 17th did not indicate the presence of elevated ozone or precursor layers aloft, so absent data for the 5–7 September period, clean air conditions aloft were prescribed for both modeling episodes.

Boundary conditions were developed from analysis of the routine air quality monitoring data, the hydrocarbon sampling results, and the range of boundary conditions used in previous UAM modeling studies in coastal California settings. The values chosen, presented in Table 4, are a midrange estimate of background tropospheric concentrations.

Wind observations in the eastern basin (Piru and Simi) on the 6th and 7th indicated precursor transport into the SCCAB from the adjacent San Fernando Valley and the south coast air basin. Hourly air quality data from the 5–7 September for the Burbank and Re-

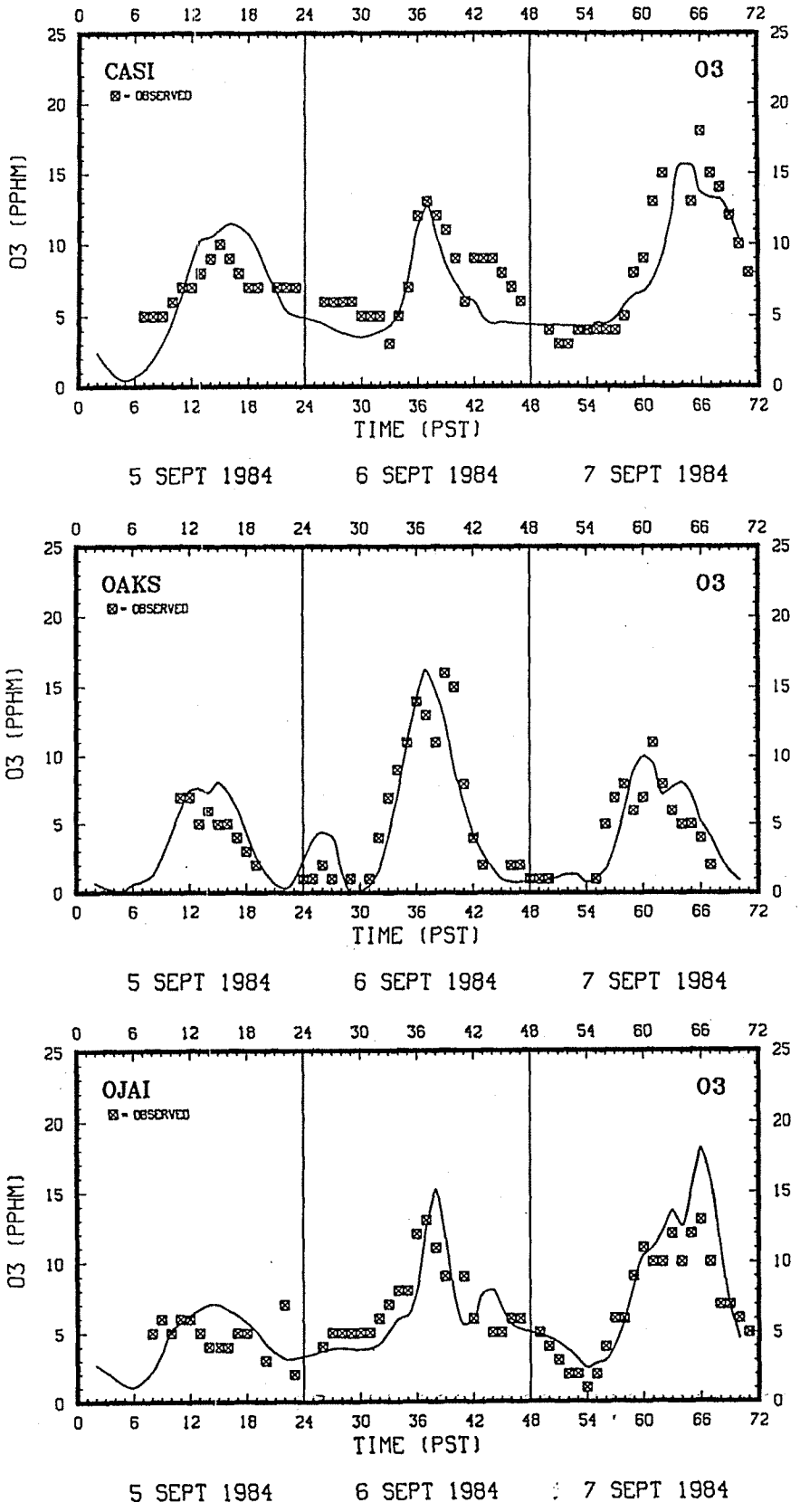

FIG. 3. Estimated and observed hourly averaged ozone concentrations for 5–7 September 1984 at: (a) Casitas, (b) Thousand Oaks, (c) Ojai, (d) Piru, (e) Santa Barbara, (f) Simi.

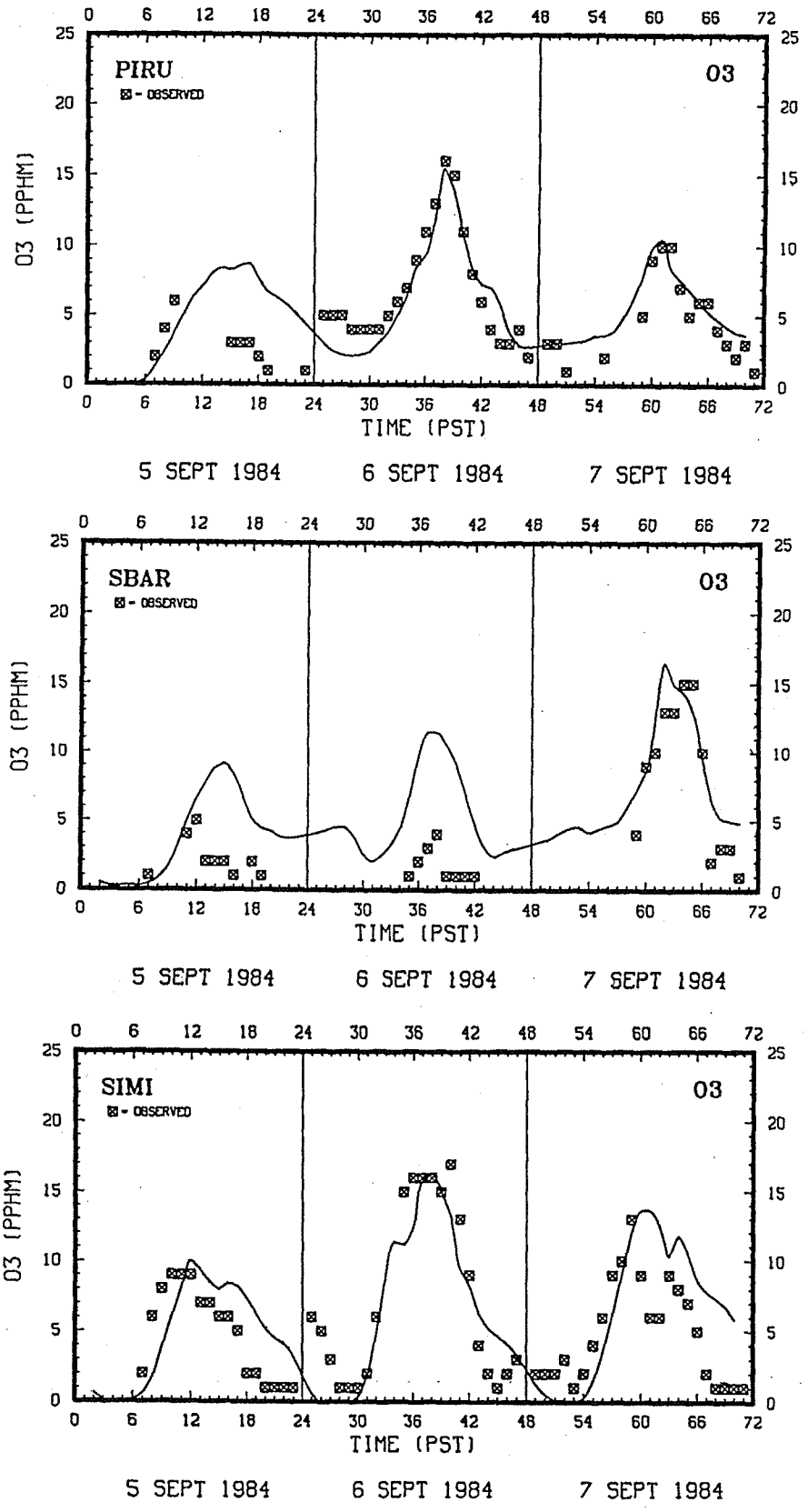

FIG. 3. (*Continued*)

seda stations in San Fernando Valley were obtained to prescribe boundary conditions in this region. We also examined the hourly concentrations near the eastern and southeastern portions of the present grid that were estimated in previous UAM modeling studies for the south coast air basin (Tesche et al. 1984). The resultant boundary conditions summarized in Table 5 only affect model calculations when the wind is directed into the computational domain, usually during the nighttime and morning hours.

Ambient hydrocarbon data were collected in evacuated canisters at numerous locations during the 1984 field program. This information was used in setting boundary conditions for hydrocarbons as well as for determining the splitting factors needed to apportion the reactive organic gas concentrations into the five CBM-II species categories. Because no speciated hydrocarbon sampling was performed for 5–7 September, we used the average splits from the 12 measurement days as an estimate for the 5–7 September episode. Day-specific splits were used for 16–17 September. The splitting factors are listed in Table 6. These values were used to distribute the estimated boundary ROG value (0.029 ppmC) into the five categories.

5. Photochemical model performance evaluation

One of the primary reasons for conducting a performance evaluation is to determine whether the model performs well enough to be used for regulatory purposes. As yet, no definitive guidelines for model performance evaluations exist despite nearly 20 years of research in this field (Tesche et al. 1991). In section 6 we discuss the SCCCAMP 1984 model evaluation results using commonly employed evaluation procedures. However, to stimulate development of a consistent process for model performance evaluation in the future, we offer a few suggestions here on the approach to model performance evaluation that should be considered in subsequent studies.

Model performance evaluation is the process of testing a model's ability to estimate accurately observed measures of air quality over a range of meteorological, emissions, and air quality conditions. It focuses and directs the continuing cycle of model development, data collection, model testing, diagnostic analysis, refinement, and retesting. While a single evaluation cannot "validate" a model, it can raise serious doubts about a model's adequacy.

Performance evaluation has several components. The *operational evaluation* is an assessment of a model's ability to estimate the correct answer whether or not the process descriptions in the model are accurate. It is an examination of how well a model reproduces observed concentration fields in time and space consistent with the needs of policy analysis or regulatory decision making. Current statistical tests and methods used in operational evaluations of urban- and regional-scale models are described by Barchet (1987), Daly et al. (1988), Dennis et al. (1989), and Tesche et al. (1991). These studies suggest specific statistical and graphical techniques for operational performance evaluation, emphasizing the use of concentration residuals to estimate model accuracy and precision. Op-

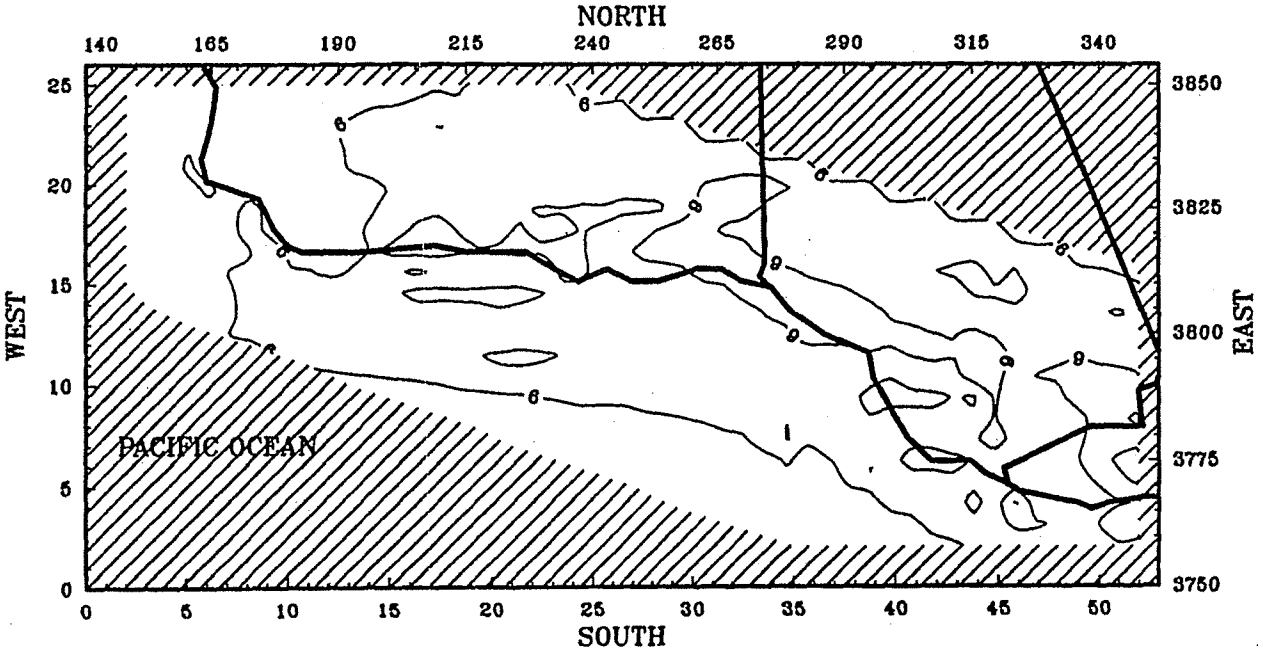

FIG. 4. Ground-level ozone estimates (pphm) between the hours of 1400 and 1500 PST 5 September 1984.

erational testing of the entire modeling system gives little, if any information about whether the results are correct from a scientific perspective or whether they are simply the fortuitous product of compensatory errors. Therefore, a "successful" operational evaluation is a necessary but insufficient condition for achieving a sound modeling exercise.

The *scientific evaluation* seeks to determine whether the model's behavior, in the aggregate and in its component modules, is consistent with prevailing theory, knowledge of physical and chemical processes, and observations. The scientific evaluation consists of several diagnostic and mechanistic tests and procedures, some of which can be prescribed in advance while others must be defined through the investigative process. These procedures have a common set of objectives, namely to: (a) identify the presence and severity of hidden or compensatory errors, (b) determine the causes of failure of a flawed model, (c) "stress" a model to ensure failure if indeed the model is flawed, and (d) provide additional insight into model performance beyond that supplied through the routine, operational evaluation procedures. "Stressing a model" is designing and carrying out performance tests that cause a model to reveal its flaw and weaknesses if it is indeed inadequate. Stressful testing is intended to reduce (or avoid) the risks associated with "weak" or otherwise inadequate tests, wherein a model is not challenged sufficiently to reveal its flaws and weaknesses or appears to be performing acceptably despite significant inadequacies in formulation or inputs.

The scientific evaluation should be carried out in three stages—diagnostic, mechanistic, and comparative. *Diagnostic evaluation* consists of an assessment of a model's ability, when functioning as a whole, to simulate processes or characteristics of the system occurring during a photochemical episode (e.g., emissions, dispersion patterns, deposition rates). The tests are chosen to challenge the science in the model. Specific focus is on detailed examination of how well individual components of the model (or modules) simulate actual atmospheric processes. *Mechanistic evaluation* is an assessment of an individual modules' ability to reproduce the observed salient features of the processes it is intended to describe. When applied to all process modules that constitute the full model, mechanistic evaluation represents a test of the correctness of the underlying science. Finally, *comparative evaluation* refers to the intercomparison between different simulation models or modules (e.g., wind field generators, mixing-height algorithms, travel demand models, motor vehicle emissions factor modules, chemical kinetic mechanisms) using observed, valid data as the standard against which the intercomparisons are judged.

For the most part, our evaluation of the 1984 SCCCAMP episodes is operational. Insufficient data were collected to support detailed diagnostic, mechanistic, or comparative evaluations. Measurement data for species other than ozone were too sparse to support detailed multispecies evaluations. Only limited data were collected that might be used to test meteorological models for wind or mixing-height estimation and no data were gathered for emissions, deposition, or chemical mechanism testing. Notwithstanding these limitations, the 1984 SCCCAMP database does offer an

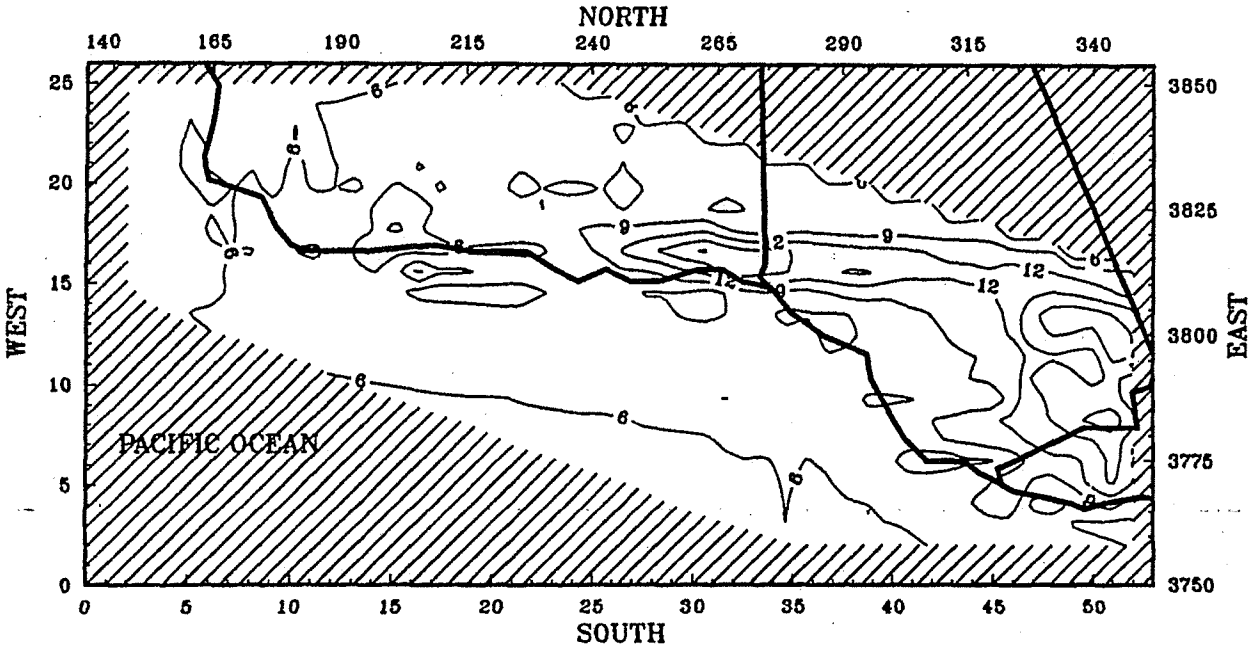

FIG. 5. Ground-level ozone estimates (pphm) between the hours of 1400 and 1500 PST 6 September 1984.

opportunity to carry out a reasonably detailed operational evaluation. The principal results of this analysis are discussed next; full details are presented in the project reports.

6. Results of the performance evaluations

a. 5–7 September 1984

A 66-h simulation of the 5–7 September 1984 ozone episode was carried out beginning at 0200 PST on the 5th. Ozone time series plots at six monitoring stations representative of high ozone locations during the 3-day period are shown in Fig. 3. The solid line represents the modeled hourly averaged ozone concentrations (pphm) in the grid cell containing the monitoring station. The boxes correspond to the hourly averaged ozone observations. As indicated in Table 1, the maximum observed ozone concentration on the 5th was 10 pphm at Casitas while the peak values on the following two days were significantly higher, with ozone maxima of 17 pphm (Simi) and 18 pphm (Casitas) on the 6th and 7th, respectively. As shown in Fig. 3a, the UAM estimated a peak of 12 pphm at Casitas on the 5th, one hour after the time of maximum reported ozone. With the exception of the Santa Barbara monitoring station, the peak concentrations on the 6th are fairly well reproduced. On the 7th, the diurnal profiles reproduce the main features of the observations. There are obvious underestimation problems at some of the stations, particularly during the nighttime and early morning hours.

Figures 4–6 present hourly averaged ground-level ozone isopleths (in pphm) at 1400 PST on the 5–7 September. The shaded region represents those portions of the UAM grid excluded from model calculations to reduce CPU time. On the 5th, an elongated, narrow region of moderate (9 pphm) ozone concentrations is simulated along a northwest–southeast axis from Santa Barbara to Moorpark. On the 6th, a localized region of high ozone (16 pphm) is simulated in the elevated terrain of the Santa Ynez Mountains northeast of the city of Santa Barbara. Based on backward (in time) trajectory analyses, this ozone "cloud" appears to have had its origin earlier in the episode from aged air parcels located over the Santa Barbara Channel and from urban emissions in the Santa Barbara–Goleta region. Farther inland, another area of elevated ozone is simulated on the 6th in the subregion surrounding Piru and Simi. Backward trajectory analyses indicate that this ozone cloud likely has had its origin over the urbanized region along the Ventura County coast. On the 6th and 7th, the modeled ozone cloud in Santa Barbara County appears to be displaced slightly to the north compared with the surface measurements. Figure 6 indicates that on the 7th, distinct subregions of high ozone are also simulated, again in the eastern portions of each county. However, the locations of the maximum ozone impacts on the 7th are shifted westward somewhat compared with the 6th.

The maximum observed ozone concentration the 7th is 18 pphm at Casitas, yet the maximum estimated value is 12.6 pphm. Examination of the ground-level concentration fields indicates that higher ozone concentrations are estimated a few grid cells to the north of the Casitas monitor. A similar, though less pronounced, shift in estimated and observed ozone fields

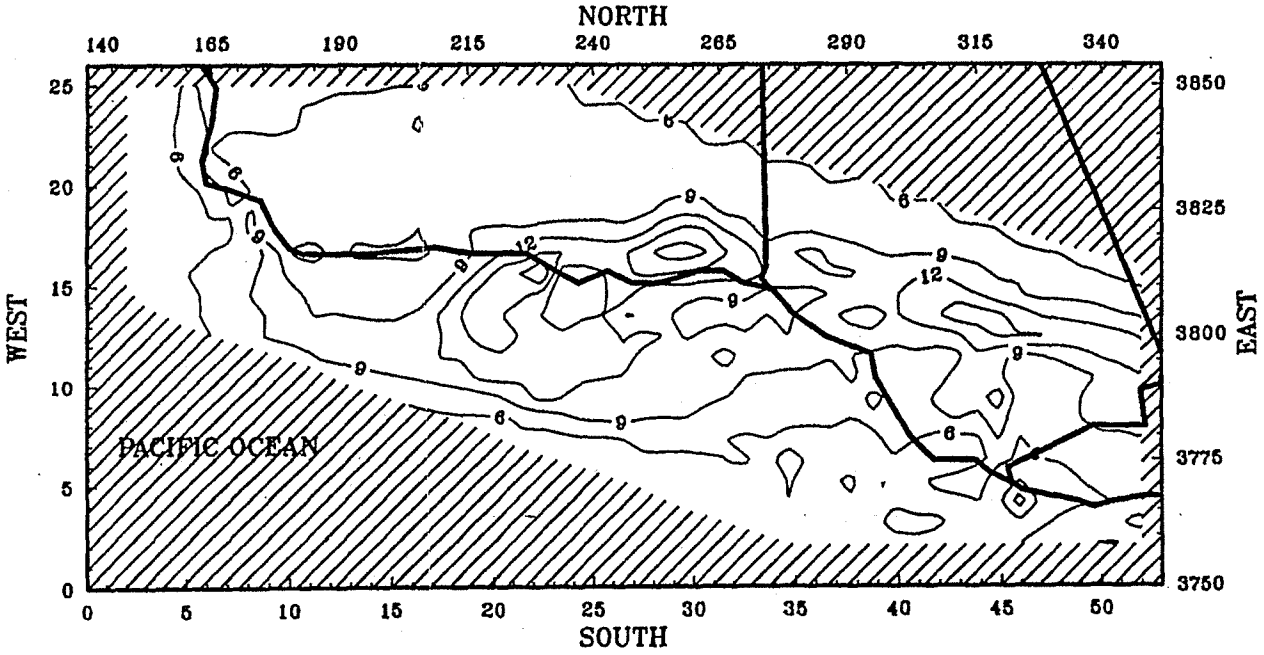

FIG. 6. Ground-level ozone estimates (pphm) between the hours of 1400 and 1500 PST 7 September 1984.

TABLE 7. Model performance in simulating maximum 1-h ozone concentrations for the 5–7 September 1984 episode (concentrations in pphm).

	5 September			6 September			7 September		
Monitoring station	Observed concentration	Predicted concentration	Percentage difference	Observed concentration	Predicted concentration	Percentage difference	Observed concentration	Predicted concentration	Percentage difference
ELRO	4.0	7.3	82	6.0	8.2	36	7.0	8.2	18
SIMI	9.0	10.0	11	17.0	16.3	−4	13.0	13.7	5
SBAR	5.0	9.2	84	4.0	11.5	187	15.0	16.5	10
CASI	10.0	12.0	20	13.0	9.9	−24	18.0	12.6	−30
PIRU	6.0	8.7	45	16.0	15.5	−3	10.0	10.5	5
OJAI	7.0	7.0	0	13.0	15.2	17	13.0	18.1	39
OAKS	7.0	8.2	17	16.0	16.3	2	11.0	10.0	−9
ELCP	5.0	6.5	31	10.0	6.2	−38	11.0	13.4	22
GOLA	7.0	6.7	−4	8.0	9.0	12	15.0	14.2	−5
VBGW	4.0	3.8	−5	4.0	4.8	19	6.0	6.0	−1
VBGH	3.0	4.1	37	3.0	4.9	64	6.0	5.7	−6
SYNZ	6.0	8.3	38	4.0	7.1	78	8.0	7.7	−4
LOMH	3.0	5.6	87	3.0	6.8	125	6.0	7.1	19
GAVI	8.0	6.3	−22	6.0	6.5	9	13.0	10.3	−21
Avg	6.0	7.4		8.8	9.9		10.9	11.0	

is apparent in the vicinity of the Ojai monitor. Here, the model estimates a peak value of 18.1 pphm (compared to an observed peak of 13 pphm) while a few grid cells away the model estimates values equal to or greater than the observations. Thus, near these monitoring stations, UAM estimates are comparable to the maximum values observed, but the spatial offset of the modeled ozone cloud produces a 5 pphm underestimation at one site (Casitas) and a 5 pphm overestimation at the other (Ojai) when the estimates and observations are matched in time and space.

Maximum observed and estimated hourly averaged ozone concentrations at each monitoring station for the three simulation days are listed in Table 7. For 5 September, the average observed ozone maximum is 6.0 pphm, compared with a peak average value of 7.4 pphm. On the 6th, the ozone peaks at Simi and Piru were underestimated by −4% and −3%. At Thousand Oaks, the peak was overestimated by 2% on the 6th. The peak estimation performance on the 7th is somewhat poorer. The maximum observed value of 18 pphm at Casitas was underestimated by 30%. However, the average peak model estimate over all 14 monitoring stations was nearly identical to the average measured value (10.9 pphm vs 11.0 pphm).

The accuracy of peak ozone concentrations may be described in several ways. The 6 September ozone results shown in Table 7 may be used to exemplify three methods. A stringent method is to compute the spatially paired accuracy of the peak model estimate. This is based on the maximum observed ozone value in the basin on the 6th (17 pphm at Simi) and the maximum estimated value at the same location (16.3 pphm), but not necessarily at the same hour. This measure of accuracy is −4%. Another method gives the "unpaired accuracy of the peak estimate." This is computed with

TABLE 8. Airshed model ozone performance statistics for the two September 1984 simulations (concentrations greater than or equal to 4 pphm).

Performance measure	5 September	6 September	7 September	16 September	17 September
Maximum estimated station ozone concentration (pphm)	12.0 (Casi)	16.3 (Simi)	18.1 (Ojai)	11.0 (Piru)	12.5 (Ojai)
Maximum observed ozone concentration (pphm)	10.0 (Casi)	17.0 (Simi)	18.0 (Casi)	11.0 (Simi)	14.0 (Casi)
Ratio of estimated to observed maxima	1.201	0.961	1.004	1.000	0.891
Accuracy (paired) of peak estimation (percent)	+20%	−4%	−30%	0%	18%
Accuracy (unpaired) of peak estimate (percent)	+20%	−4%	−30%	0%	11%
Mean normalized deviation (bias)	+0.108	−0.056	0.036	0.093	−0.046
Mean absolute normalized deviation (error)	0.377	0.324	0.234	0.264	0.262

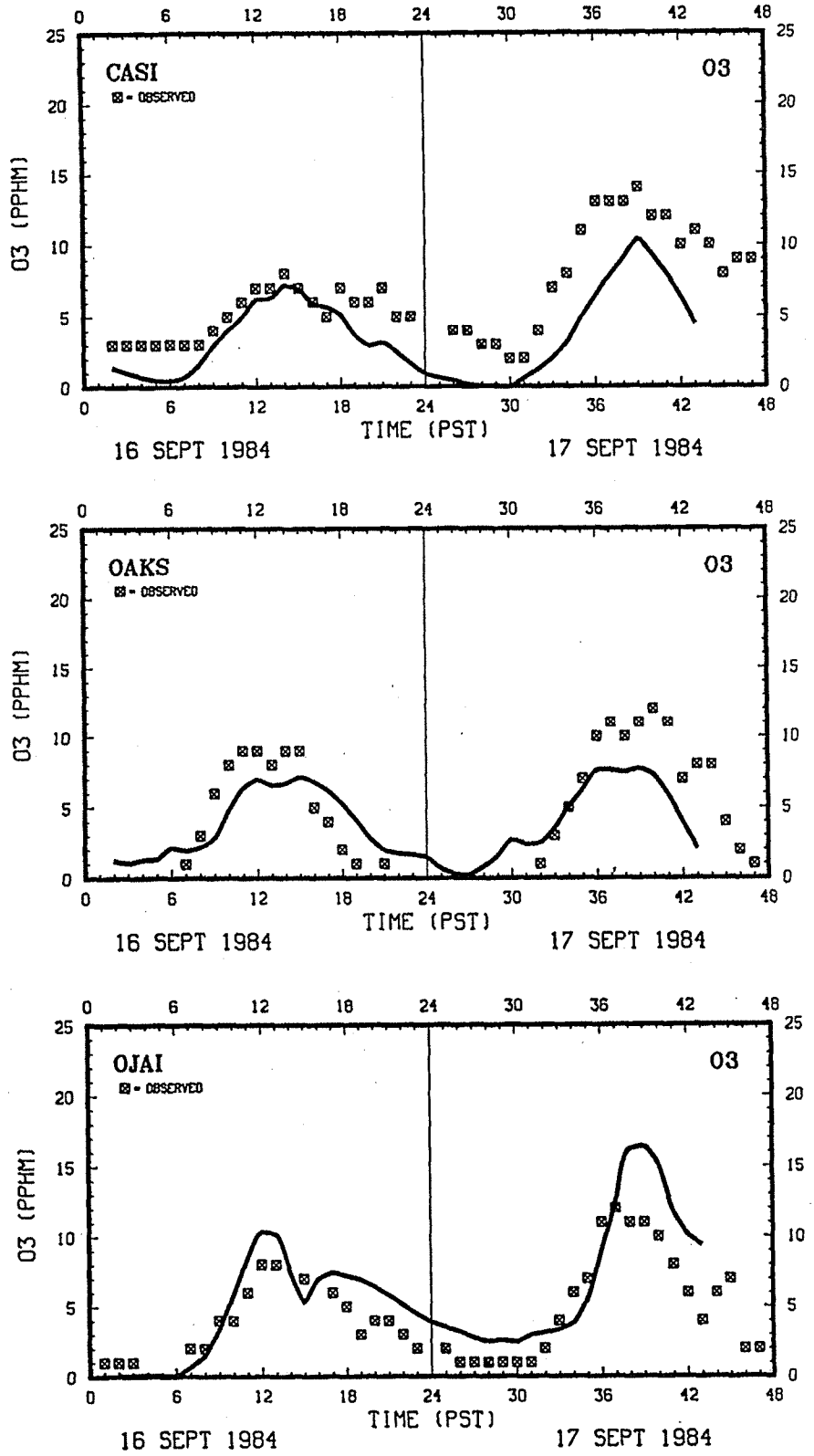

FIG. 7. Estimated and observed hourly averaged ozone concentrations for 16–17 September 1984 at: (a) Casitas, (b) Thousand Oaks, (c) Ojai, (d) Piru, (e) Santa Barbara, (f) Simi.

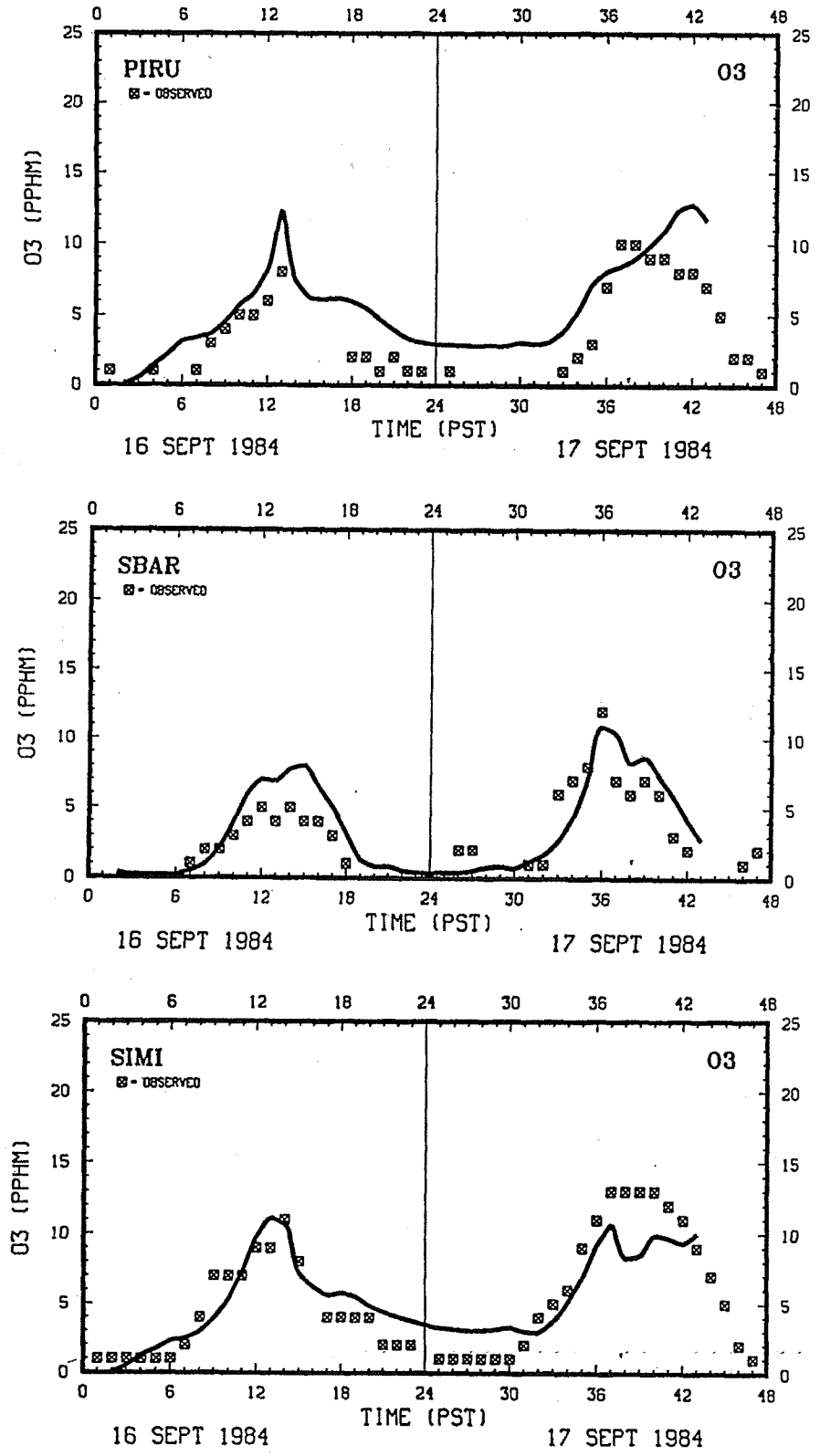

FIG. 7. (*Continued*)

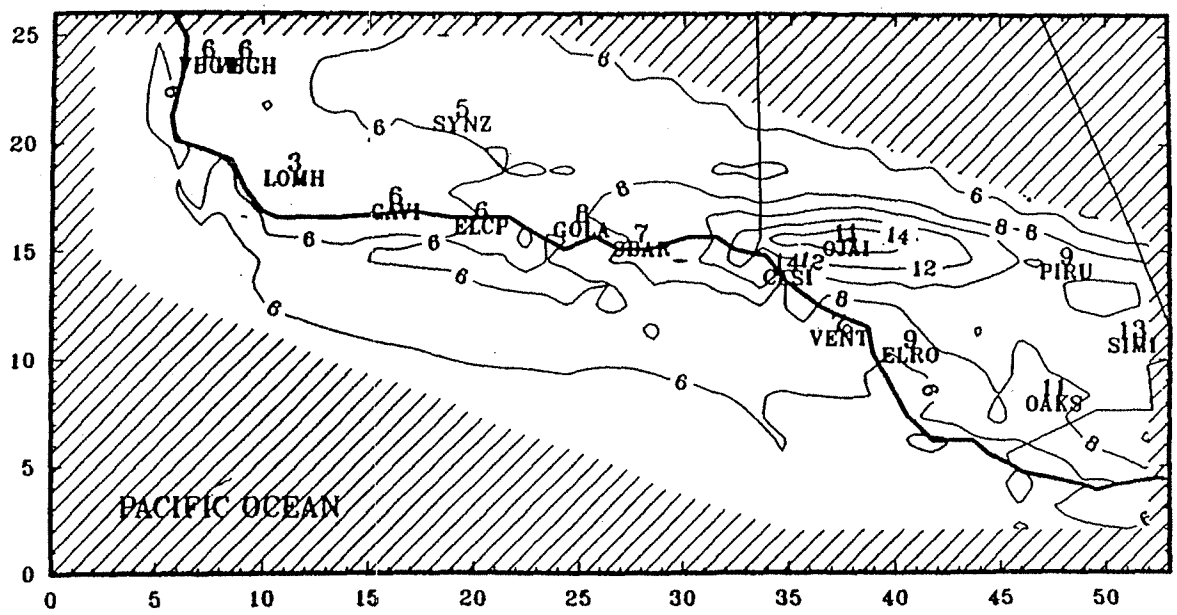

FIG. 8. Ground-level ozone estimates (pphm) between the hours of 1500 and 1600 PST 17 September 1984.

the basin maximum of 17 pphm at Simi and the highest ozone estimate of *any* of the monitoring stations in the basin. In this case, the highest estimated value is 16.3 pphm at Thousand Oaks and Simi, which leads to the same numerical value as before, −4%. The third method involves computing the spatially paired accuracies of peak estimation at each monitoring station (above 4 pphm) and then averaging the results to yield the "average of the station peak estimation accuracies." For the three simulation days, these averages are 27%, 16%, and 14%, respectively. Each of these measures of accuracy provide some insight into the modeling results but they need to be considered in the broader context of two other important residual measures—bias and error.

Table 8 presents the bias and error statistics for the 5–7 September episode. Bias is computed as the average of the signed residuals of the model estimate–observation pairs normalized by the observed concentration. This quantity is calculated using all residual pairs (all hours and all monitors) for which the observed ozone values equal or exceed 4 pphm. The gross error is com-

TABLE 9. Model performance in simulating maximum 1-h ozone concentrations for the 16–17 September 1984 episode (concentrations in pphm).

	16 September			17 September		
Monitoring station	Observed maximum concentration	Predicted maximum concentration	Percentage difference	Observed maximum concentration	Predicted maximum concentration	Percentage difference
ELRO	6.0	7.5	24	10.0	8.4	−16
SIMI	11.0	10.9	−1	13.0	10.7	−18
VENT	7.0	7.9	12	10.0	8.0	−21
SBAR	5.0	6.8	35	12.0	11.1	−8
CASI	8.0	7.6	−5	14.0	11.5	−18
PIRU	8.0	11.6	37	10.0	12.3	23
OJAI	8.0	10.2	27	12.0	12.5	4
OAKS	9.0	7.5	−17	12.0	9.3	−23
ELCP	6.0	6.1	1	6.0	6.8	14
GOLA	6.0	6.5	9	11.0	8.6	−22
VBGW	5.0	5.0	0	6.0	5.1	−14
VBGH	6.0	5.3	−11	6.0	5.3	−12
SYNZ	5.0	6.8	36	6.0	6.5	8
LOMH	5.0	5.9	17	4.0	5.5	37
GAVI	4.0	4.8	19	7.0	5.5	−22
Avg	6.6	7.3		9.3	8.5	

puted from the mean absolute normalized residual. The UAM overestimates ozone levels by 10.8% on the 5th and the overall gross error is 37.7%. This error is relatively high, in part because the concentrations on the 5th are generally low; thus, the denominators in the error calculation are typically smaller numbers compared with the 6th and 7th. On the 6th, there is a small bias toward underestimation, −5.6%. On the 7th, the bias is +3.6%. The gross errors on the 6th and 7th are 32.4% and 23.4%, respectively.

b. 16–17 September 1984

Time-series plots of estimated and observed ozone concentrations at the six monitoring stations for the 16–17 September 1984 simulation are given in Fig. 7. The model does better in reproducing the 16th's ozone levels compared with the 5th. On the 17th, the model overestimates at some stations and underestimates at others. Figure 8 is the ground-level ozone isopleth at 1500 PST on 17 September. As with the previous episode, a region of high ozone concentrations (16 pphm) is simulated north of Ojai in the elevated terrain of the Santa Ynez Mountains.

Table 9 lists the peak hourly ozone estimates and observations for this episode. On the 16th, the highest observed value is 11 pphm at Simi. The model estimates a concentration of 10.9 pphm at Simi, giving an error of −1%. The maximum estimated value, 11.6 pphm at Piru, gives an unpaired accuracy of peak estimation of +5%. The average peak estimation error over all monitoring stations on the 16th is 11%. On the 17th, the maximum observed ozone concentration is 14 pphm at Casitas. The peak estimate at the same location is 11.5 pphm, giving a peak estimation accuracy of −18%. The unpaired accuracy of peak estimation for the 17th is −11%. Considering the peak accuracy over all stations, the model shows a very slight tendency to underestimate on the 17th with value of −9%.

Table 8, introduced earlier, gives ozone bias and error estimates for the 16–17th episode also. The model overestimates hourly concentrations by 9.3% on the 16th and underestimates them by −4.6% on the 17th. Gross errors for ozone are 26.4% and 26.2%, respectively, for the two days.

7. Discussion

The evaluation statistics we have calculated for the two 1984 SCCCAMP ozone episodes are typical of the accuracy, bias, and error results reported in similar urban-scale photochemical modeling studies (Tesche 1988). It is tempting to claim that these results confirm that the model is operating properly but there are at least three reasons why we believe that just the opposite should be suspected, pending further investigation.

First, simply because the model produces results comparable to a host of previous evaluations does not demonstrate reliable performance. The definition, calculation, and reporting of performance measures has varied widely among modeling groups; no consistent evaluation methodology has been employed. Few, if any, of the previous studies, carried out a sufficiently robust set of diagnostic and mechanistic analyses to confirm that the accuracy, bias, and error statistics reported truly meant that the models were operating properly. Absent important diagnostic tests (e.g., multispecies comparisons) and mechanistic evaluations, it may be that previous photochemical model evaluations were inadvertently "tuned" to the observed ozone values.

Second, it is quite likely that hidden, or compensatory errors exist within the present model simulations that have not been revealed through the operational evaluation. For example, we previously noted the absence of detailed upper-air information with which to evaluate the performance of the mixing-height algorithms. It is conceivable that the mixing heights could be systematically underestimated. If so, this bias would produce higher ozone concentrations for both episodes based on our detailed mixing-height sensitivity experiments (Tesche et al. 1988b). Conversely, the on-hydrocarbon emission inventories are generally thought to be biased low (Seinfeld 1988), which will cause the model to underestimate ozone. Thus, the effects of mixing heights that are too low could compensate for the underestimation in hydrocarbon emissions to produce ozone concentrations that appear to be correct but for the wrong reason. A major objective of the scientific performance evaluation is to locate and quantify the magnitude of compensatory errors through a series of successively more stressful tests. Performance of these mechanistic and diagnostic tests requires sets of measurements that were not intended to be part of the 1984 SCCCAMP Exploratory Field Study.

Third, while there is a rich history of photochemical model performance evaluation using past ozone episodes, there has been very little work done to evaluate the reasonableness of ozone estimates when models are used to simulate the effects of control strategies in future years. Ideally, the adequacy of a photochemical model in correctly estimating the effects of emission changes on ambient air quality should be evaluated directly by examining model performance for applications involving significantly altered emission strengths and spatial patterns. Such an evaluation should be performed with emission estimates for the same region that correspond to years sufficiently separate in time. Since such a procedure is most likely impractical, as an alternative, one should evaluate the model for two or more different regions, using input data of comparable quality.

These limitations do not preclude the use of the 1984 episodes in designing and testing emissions control strategies. Rather, they should be carefully considered when devising control strategies and interpreting sim-

ulation results since the risks raised by compensating errors are increased.

One concern we were not able to address adequately in this study involves the use of three different models to apply wind, temperature, and mixing-height fields. The use of separate model input preprocessor programs to generate components of the meteorological fields raises the potential for dynamic and thermodynamic inconsistencies in the transport and thermal fields. Since this approach is commonly used today in urban- and regional-scale photochemical modeling, the potential significance of these inconsistencies should be investigated.

8. Conclusions

The 1984 SCCCAMP Exploratory Field Study provides useful photochemical modeling episodes in the south-central coast air basin. Two periods, 5–7 September and 16–17 September 1984, have been simulated, providing a technical basis for Santa Barbara County's Air Quality Attainment Plan and the EPA's Federal Implementation Plan for Ventura County. An operational ozone model performance evaluation was performed for the 5–7 and 16–17 September 1984 episodes. The UAM reproduced the peak 1-h ozone concentrations (paired in time and space) on the five simulation days with accuracies ranging from 0% to −30%. The average bias, the tendency to over- or underestimate hourly averaged ozone concentrations, ranged between −6% and +11%. The average gross errors in hourly estimates varied between 23% and 38%. UAM performance in simulating hourly averaged ozone concentrations for both episodes is found to compare well with other recent photochemical model evaluations in the United States.

The major limitation of the present evaluation study involves the absence of detailed diagnostic and mechanistic analyses. The 1984 SCCCAMP database was not designed to support a scientific model performance exercise so data essential for multispecies evaluations, testing of individual model components such as windfields, emissions, deposition, or chemistry, and for performing compensatory error analyses are not collected. Consequently, decision-makers must exercise caution in the interpretation of emission control scenarios derived from the 5–7 September and 16–17 September 1984 databases since these important evaluative tests were not carried out.

A pressing challenge in photochemical model evaluation today is the need to devise and implement more rigorous techniques for revealing the presence and effects of compensatory errors in model simulations. Meeting this challenge will require thoughtful construction of a set of stress tests that may be applied to the entire modeling system as well as to its component parts. Unfortunately, even the most intensive databases currently available have important limitations. Detailed stress testing and compensatory error analysis will necessitate the collection of new, highly specialized databases. Ultimately, public policy makers will have to decide: (a) just how important the answers to the questions raised in section 1 are to them, in terms of supporting their decision-making needs, (b) and just how much money is appropriate to spend for data collection and modeling analyses to obtain these answers.

Acknowledgments. The authors express their appreciation to Mr. John Vimont of the U.S. EPA Region IX; Mr. Andrew J. Ranzieri and Dr. Kit Wagner of the California Air Resources Board; Dr. Savithri Machiraju, formerly of the Santa Barbara County Air Pollution Control District; and Mr. Evan Shipp of the Ventura County Air Pollution Control District for their assistance and technical input throughout this study. Particularly helpful insight regarding model performance evaluation was offered by Dr. Philip M. Roth. Dr. Walt Dabberdt of the National Center for Atmospheric Research and two anonymous reviewers are also thanked for their constructive suggestions.

REFERENCES

Ames, J., T. C. Meyers, L. E. Reid, D. C. Whitney, S. H. Golding, S. R. Hayes and S. D. Reynolds, 1985: SAI airshed model operations manuals: Volume I—user's manual. Rep. by Systems Applications, Inc., San Rafael, CA., EPA-68-02-2429, 265 pp.

Barchet, W. R., 1987: Evaluation of regional-scale air quality-models: Chairman reps. from four workshops. Electric Power Research Institute, Research Project 1630-40, 153 pp. [Available from Battelle Pacific Northwest Laboratories, Richland, WA.]

Dabberdt, W. F., 1984: Preliminary summary of the 1984 South-Central Coast Cooperative Aerometric Monitoring Program (SCCCAMP) exploratory study. 71 pp. [Available from SRI, Altadena, CA.]

——, and W. Viezee, 1987: South Central Coast Cooperative Aerometric Monitoring Program (SCCCAMP). *Bull. Amer. Meteor. Soc.*, **68**, 1098–1110.

Daly, C., M. A. Yocke, R. L. Dennis, S. Seilkop and P. M. Roth, 1988: Protocol for evaluating the predictive performance of the regional acidic Deposition Models RADM and ADOM. Environmental Protection Agency 68-02-4129, Atmospheric Sciences Research Laboratory, Research Triangle Park, NC, 127 pp.

Dennis, R. L., W. R. Barchet, T. L. Clark, S. K. Seilkop and P. M. Roth, 1989: Evaluation of regional acid deposition models. State-of-Science Tech. Rep. No. 5, National Acid Precipitation Assessment Program, Washington, D.C., 187 pp.

Environmental Protection Agency, 1986: Guideline on air quality models (Revised). EPA-450/2-78-027R, United States Environmental Protection Agency, Office of Air Quality Planning and Standards, Research Triangle Park, NC, 137 pp..

Gery, M. W., G. Z. Whitten and J. P. Killus 1988: Development and testing of the CBM-IV for urban and regional modeling. EPA/600/3-88/012, United States Environmental Protection Agency, Research Triangle Park, NC, 137 pp.

Goodin, W. R., G. J. McRae and J. H. Seinfeld, 1980: An objective analysis technique for constructing three-dimensional urban-scale wind fields. *J. Appl. Meteor.*, **19**, 96–106.

Haney, J. L., D. R. Souten, T. W. Tesche, L. R. Chinkin, H. Hogo and M. C. Dudik, 1986: Evaluation and Application of the PARIS photochemical model in the South Central Coast Air Basin, SYSAPP-86/065 Rep. by Systems Applications, 383 pp. [Available from United States Environmental Protection Agency.]

Holtslag, A. A. M., and A. P. van Ulden, 1983: A simple scheme for daytime estimates of the surface fluxes from routine weather data. *J. Climate Appl. Meteor.*, **22,** 517–529.

Kessler, R. C., and S. G. Douglas, 1989: Numerical simulation of mesoscale airflow in the South Central Coast Air Basin. SYSAPP-89/077, Final Rep., 252 pp. [Available from Systems Applications, Inc., San Rafael, CA.]

Morris, R. E., T. C. Myers and J. L. Haney, 1990: User's guide for the urban airshed model: Volume I. User's manual for UAM (CB-IV). Report by Systems Applications, Inc., No. SYSAPP-90/018a, 259 pp. [Available from U.S. Environmental Protection Agency, Office of Air Quality Planning and Standards, Research Triangle Park, NC.]

Reynolds, S. D., T. W. Tesche and D. R. Souten, 1985: Overall study protocol for the South Central Coast Cooperative Aerometric Monitoring Program. Final Rep. to the Western Oil and Gas Association, 287 pp. [Available from Systems Applications, Inc., San Rafael, CA.

Seinfeld, J. H., 1988: Ozone air quality models: a critical review. *J. Air Pollut. Control Assoc.*, **38,** 616–645.

SLC, 1986: Environmental impact rep. environmental impact statement for proposed ARCO coal oil point project: Appendix 4—air quality—meteorology: Volume II. [Available from California State Lands Commission, Sacramento, CA.]

Smolarkiewicz, P. K., 1983: A simple positive definite advection scheme with small implicit diffusion. *Mon. Wea. Rev.*, **111,** 479–486.

Stauffer, D. R., and N. L. Seaman, 1990: Use of four-dimensional data assimilation in a limited-area mesoscale model. *Mon. Wea. Rev.*, **118,** 1250–1277.

Steyn, D. G., and T. R. Oke, 1982: The depth of the daytime mixed layer at two coastal sites: A model and its validation. *Bound. Layer Meteor.*, **24,** 161–180.

Tennekes, H., 1973: A model for the dynamics of the inversion above the convective boundary layer, *J. Atmos. Sci.*, **30,** 558–567.

Tesche, T. W., 1988: Accuracy of ozone air quality models. *J. Environ. Eng.*, **114,** 739–752.

——, 1991: Evaluating procedures for using numerical meteorological models as input to photochemical models. *7th Joint Conference on Applications of Air Pollution Meteorology,* New Orleans, Amer. Meteor. Soc., 6 pp.

——, and D. E. McNally, 1989: Urban airshed modeling in support of the ventura ozone federal implementation plan. Rep. to the United States Environmental Protection Agency, Region IX, EPA Contract No. 68-02-4392, Work Assignment No. 37, 97 pp.

——, C. Seigneur, B. Oliver and J. L. Haney, 1984: Modeling ozone control strategies in Los Angeles. *J. Environ. Eng.*, **110,** 208–225.

——, C. Daly, B. D. Miller and S. D. Reynolds, 1985: Analysis of the data collected in the 1984 SCCCAMP field program. SYSAPP-85/029, Final Program Rep. to the South-Central Coast Cooperative Aerometric Monitoring Program, 208 pp. [Available from Systems Applications, Inc., San Rafael, CA.]

——, J. G. Wilkinson, D. E. McNally, R. Kapahi and B. Oliver, 1988a: Photochemical modeling of two SCCCAMP 1984 oxidant episodes: Volume 11: Modeling procedures and evaluation results, Final Program Rep. to the United States Environmental Protection Agency, Region IX, San Francisco, CA, 352 pp.

——, D. E. McNally and J. G. Wilkinson, 1988b: Importance of boundary layer measurements for urban airshed modeling. *81st Modeling of the Air Pollution Control Association,* Dallas, 18 pp.

——, P. Georgopoulos, J. H. Seinfeld, P. M. Roth, F. W. Lurmann and G. Cass, 1990: Improvement of procedures for evaluating photochemical models. Final Rep. to the California Air Resources Board, Contract No. A832-103, Sacramento, CA, 352 pp.

van Ulden, A. P., and A. A. M. Holtslag, 1985: Estimation of atmospheric boundary layer parameters for diffusion applications. *J. Climate Appl. Meteor.*, **24,** 1196–1207.

Wagner, K. K., 1989: Evaluation of NO_x and reactive hydrocarbon emission controls for ozone in the South Central Coast Air Basin of California. *82nd Annual Meeting of the Air and Waste Management Association,* Anaheim, CA, 9 pp.

Whitten, G. Z., H. Hogo and J. P. Killus, 1980: The carbon-bond mechanism: A condensed kinetic mechanism for photochemical smog. *Environ. Sci. Technol.*, **14,** 657–682.

Wilczak, J. M., and M. S. Phillips, 1986: An indirect estimation of convective boundary layer structure for use in pollution dispersion models. *J. Climate Appl. Meteor.*, **25,** 1069–1624.

3.2 Natural Gas-fired Reciprocating Engines

3.2.1 General[1-3]

Most natural gas-fired reciprocating engines are used in the natural gas industry at pipeline compressor and storage stations and at gas processing plants. These engines are used to provide mechanical shaft power for compressors and pumps. At pipeline compressor stations, engines are used to help move natural gas from station to station. At storage facilities, they are used to help inject the natural gas into high pressure natural gas storage fields. At processing plants, these engines are used to transmit fuel within a facility and for process compression needs (e.g., refrigeration cycles). The size of these engines ranges from 50 brake horsepower (bhp) to 11,000 bhp. In addition, some engines in service are 50 - 60 years old and consequently have significant differences in design compared to newer engines, resulting in differences in emissions and the ability to be retrofitted with new parts or controls.

At pipeline compressor stations, reciprocating engines are used to power reciprocating compressors that move compressed natural gas (500 - 2000 psig) in a pipeline. These stations are spaced approximately 50 to 100 miles apart along a pipeline that stretches from a gas supply area to the market area. The reciprocating compressors raise the discharge pressure of the gas in the pipeline to overcome the effect of frictional losses in the pipeline upstream of the station, in order to maintain the required suction pressure at the next station downstream or at various downstream delivery points. The volume of gas flowing and the amount of subsequent frictional losses in a pipeline are heavily dependent on the market conditions that vary with weather and industrial activity, causing wide pressure variations. The number of engines operating at a station, the speed of an individual engine, and the amount of individual engine horsepower (load) needed to compress the natural gas is dependent on the pressure of the compressed gas received by the station, the desired discharge pressure of the gas, and the amount of gas flowing in the pipeline. Reciprocating compressors have a wider operating bandwidth than centrifugal compressors, providing increased flexibility in varying flow conditions. Centrifugal compressors powered by natural gas turbines are also used in some stations and are discussed in another section of this document.

A compressor in storage service pumps gas from a low-pressure storage field (500 - 800 psig) to a higher pressure transmission pipeline (700 - 1000 psig) and/or pumps gas from a low-pressure transmission line (500 - 800 psig) to a higher pressure storage field (800 - 2000 psig).

Storage reciprocating compressors must be flexible enough to allow operation across a wide band of suction and discharge pressures and volume variations. The compressor must be able to compress at high compression ratios with low volumes and compress at low compression ratios with high volumes. These conditions require varying speeds and load (horsepower) conditions for the reciprocating engine powering the reciprocating compressor.

Reciprocating compressors are used at processing plants for process compression needs (e.g. refrigeration cycles). The volume of gas compressed varies, but the pressure needed for the process is more constant than the other two cases mentioned above.

3.2.2 Process Description[1-3]

Natural gas-fired reciprocating engines are separated into three design classes: 2-cycle (stroke) lean-burn, 4-stroke lean-burn, and 4-stroke rich-burn. Two-stroke engines complete the power cycle in a

single crankshaft revolution as compared to the two crankshaft revolutions required for 4-stroke engines. All engines in these categories are spark-ignited.

In a 2-stroke engine, the air-to-fuel charge is injected with the piston near the bottom of the power stroke. The intake ports are then covered or closed, and the piston moves to the top of the cylinder, compressing the charge. Following ignition and combustion, the power stroke starts with the downward movement of the piston. As the piston reaches the bottom of the power stroke, exhaust ports or valves are opened to exhaust, or scavenge, the combustion products, and a new air-to-fuel charge is injected. Two-stroke engines may be turbocharged using an exhaust-powered turbine to pressurize the charge for injection into the cylinder and to increase cylinder scavenging. Non-turbocharged engines may be either blower scavenged or piston scavenged to improve removal of combustion products. Historically, 2-stroke designs have been widely used in pipeline applications. However, current industry practices reflect a decline in the usage of new 2-stroke engines for stationary applications.

Four-stroke engines use a separate engine revolution for the intake/compression cycle and the power/exhaust cycle. These engines may be either naturally aspirated, using the suction from the piston to entrain the air charge, or turbocharged, using an exhaust-driven turbine to pressurize the charge. Turbocharged units produce a higher power output for a given engine displacement, whereas naturally aspirated units have lower initial costs and require less maintenance.

Rich-burn engines operate near the stoichiometric air-to-fuel ratio (16:1) with exhaust excess oxygen levels less than 4 percent (typically closer to 1 percent). Additionally, it is likely that the emissions profile will be considerably different for a rich-burn engine at 4 percent oxygen than when operated closer to stoichiometric conditions. Considerations such as these can impact the quantitative value of the emission factor presented. It is also important to note that while rich-burn engines may operate, by definition, with exhaust oxygen levels as high as 4 percent, in reality, most will operate within plus or minus 1 air-to-fuel ratio of stoichiometry. Even across this narrow range, emissions will vary considerably, sometimes by more than an order of magnitude. Air-to-fuel ratios were not provided in the gathered emissions data used to develop the presented factors.

Lean-burn engines may operate up to the lean flame extinction limit, with exhaust oxygen levels of 12 percent or greater. The air to fuel ratios of lean-burn engines range from 20:1 to 50:1 and are typically higher than 24:1. The exhaust excess oxygen levels of lean-burn engines are typically around 8 percent, ranging from 4 to 17 percent. Some lean-burn engines are characterized as clean-burn engines. The term "clean-burn" technology is a registered trademark of Cooper Energy Systems and refers to engines designed to reduce NO_x by operating at high air-to-fuel ratios. Engines operating at high air-to-fuel ratios (greater than 30:1) may require combustion modification to promote stable combustion with the high excess air. These modifications may include a turbo charger or a precombustion chamber (PCC). A turbo charger is used to force more air into the combustion chamber, and a PCC is used to ignite a fuel-rich mixture that propagates into the main cylinder and ignites the very lean combustion charge. Lean-burn engines typically have lower oxides of nitrogen (NO_x) emissions than rich-burn engines.

3.2.3 Emissions

The primary criteria pollutants from natural gas-fired reciprocating engines are oxides of nitrogen (NO_x), carbon monoxide (CO), and volatile organic compounds (VOC). The formation of nitrogen oxides is exponentially related to combustion temperature in the engine cylinder. The other pollutants, CO and VOC species, are primarily the result of incomplete combustion. Particulate matter (PM) emissions include trace amounts of metals, non-combustible inorganic material, and condensible,

semi-volatile organics which result from volatized lubricating oil, engine wear, or from products of incomplete combustion. Sulfur oxides are very low since sulfur compounds are removed from natural gas at processing plants. However, trace amounts of sulfur containing odorant are added to natural gas at city gates prior to distribution for the purpose of leak detection.

It should be emphasized that the actual emissions may vary considerably from the published emission factors due to variations in the engine operating conditions. This variation is due to engines operating at different conditions, including air-to-fuel ratio, ignition timing, torque, speed, ambient temperature, humidity, and other factors. It is not unusual to test emissions from two identical engines in the same plant, operated by the same personnel, using the same fuel, and have the test results show significantly different emissions. This variability in the test data is evidenced in the high relative standard deviation reported in the data set.

3.2.3.1 Nitrogen Oxides -

Nitrogen oxides are formed through three fundamentally different mechanisms. The principal mechanism of NO_x formation with gas-fired engines is thermal NO_x. The thermal NO_x mechanism occurs through the thermal dissociation and subsequent reaction of nitrogen (N_2) and oxygen (O_2) molecules in the combustion air. Most NO_x formed through the thermal NO_x mechanism occurs in high-temperature regions in the cylinder where combustion air has mixed sufficiently with the fuel to produce the peak temperature fuel/air interface. The second mechanism, called prompt NO_x, occurs through early reactions of nitrogen molecules in the combustion air and hydrocarbon radicals from the fuel. Prompt NO_x reactions occur within the flame and are usually negligible compared to the level of NO_x formed through the thermal NO_x mechanism. The third mechanism, fuel NO_x, stems from the evolution and reaction of fuel-bound nitrogen compounds with oxygen. Natural gas has negligible chemically bound fuel nitrogen (although some molecular nitrogen is present).

Essentially all NO_x formed in natural gas-fired reciprocating engines occurs through the thermal NO_x mechanism. The formation of NO_x through the prompt NO_x mechanism may be significant only under highly controlled situations in rich-burn engines when the thermal NO_x mechanism is suppressed. The rate of NO_x formation through the thermal NO_x mechanism is highly dependent upon the stoichiometric ratio, combustion temperature, and residence time at the combustion temperature. Maximum NO_x formation occurs through the thermal NO_x mechanism near the stoichiometric air-to-fuel mixture ratio since combustion temperatures are greatest at this air-to-fuel ratio.

3.2.3.2 Carbon Monoxide and Volatile Organic Compounds -

CO and VOC emissions are both products of incomplete combustion. CO results when there is insufficient residence time at high temperature to complete the final step in hydrocarbon oxidation. In reciprocating engines, CO emissions may indicate early quenching of combustion gases on cylinder walls or valve surfaces. The oxidation of CO to carbon dioxide (CO_2) is a slow reaction compared to most hydrocarbon oxidation reactions.

The pollutants commonly classified as VOC can encompass a wide spectrum of volatile organic compounds that are photoreactive in the atmosphere. VOC occur when some of the gas remains unburned or is only partially burned during the combustion process. With natural gas, some organics are carryover, unreacted, trace constituents of the gas, while others may be pyrolysis products of the heavier hydrocarbon constituents. Partially burned hydrocarbons result from poor air-to-fuel mixing prior to, or during, combustion, or incorrect air-to-fuel ratios in the cylinder during combustion due to maladjustment of the engine fuel system. Also, low cylinder temperature may yield partially burned hydrocarbons due to excessive cooling through the walls, or early cooling of the gases by expansion of the combustion volume caused by piston motion before combustion is completed.

3.2.3.3 Particulate Matter[4] -

PM emissions result from carryover of noncombustible trace constituents in the fuel and lubricating oil and from products of incomplete combustion. Emission of PM from natural gas-fired reciprocating engines are generally minimal and comprise fine filterable and condensible PM. Increased PM emissions may result from poor air-to-fuel mixing or maintenance problems.

3.2.3.4 Carbon Dioxide, Methane, and Nitrous Oxide[5] -

Carbon dioxide (CO_2), methane (CH_4), and nitrous oxide (N_2O) are referred to as greenhouse gases. Such gases are largely transparent to incoming solar radiation; however, they absorb infrared radiation re-emitted by the Earth. Where available, emission factors for these pollutants are presented in the emission factors tables of this section.

3.2.4 Control Technologies

Three generic control techniques have been developed for reciprocating engines: parametric controls (timing and operating at a leaner air-to-fuel ratio); combustion modifications such as advanced engine design for new sources or major modification to existing sources (clean-burn cylinder head designs and prestratified charge combustion for rich-burn engines); and postcombustion catalytic controls installed on the engine exhaust system. Post-combustion catalytic technologies include selective catalytic reduction (SCR) for lean-burn engines, nonselective catalytic reduction (NSCR) for rich-burn engines, and CO oxidation catalysts for lean-burn engines.

3.2.4.1 Control Techniques for 4-Cycle Rich-burn Engines[4,6] -

Nonselective Catalytic Reduction (NSCR) -

This technique uses the residual hydrocarbons and CO in the rich-burn engine exhaust as a reducing agent for NO_x. In an NSCR, hydrocarbons and CO are oxidized by O_2 and NO_x. The excess hydrocarbons, CO, and NO_x pass over a catalyst (usually a noble metal such as platinum, rhodium, or palladium) that oxidizes the excess hydrocarbons and CO to H_2O and CO_2, while reducing NO_x to N_2. NO_x reduction efficiencies are usually greater than 90 percent, while CO reduction efficiencies are approximately 90 percent.

The NSCR technique is effectively limited to engines with normal exhaust oxygen levels of 4 percent or less. This includes 4-stroke rich-burn naturally aspirated engines and some 4-stroke rich-burn turbocharged engines. Engines operating with NSCR require tight air-to-fuel control to maintain high reduction effectiveness without high hydrocarbon emissions. To achieve effective NO_x reduction performance, the engine may need to be run with a richer fuel adjustment than normal. This exhaust excess oxygen level would probably be closer to 1 percent. Lean-burn engines could not be retrofitted with NSCR control because of the reduced exhaust temperatures.

Prestratified Charge -

Prestratified charge combustion is a retrofit system that is limited to 4-stroke carbureted natural gas engines. In this system, controlled amounts of air are introduced into the intake manifold in a specified sequence and quantity to create a fuel-rich and fuel-lean zone. This stratification provides both a fuel-rich ignition zone and rapid flame cooling in the fuel-lean zone, resulting in reduced formation of NO_x. A prestratified charge kit generally contains new intake manifolds, air hoses, filters, control valves, and a control system.

3.2.4.2 Control Techniques for Lean-burn Reciprocating Engines[4,6] -

Selective Catalytic Reduction[4,6] -

Selective catalytic reduction is a postcombustion technology that has been shown to be effective in reducing NO_x in exhaust from lean-burn engines. An SCR system consists of an ammonia storage, feed, and injection system, and a catalyst and catalyst housing. Selective catalytic reduction systems selectively reduce NO_x emissions by injecting ammonia (either in the form of liquid anhydrous ammonia or aqueous ammonium hydroxide) into the exhaust gas stream upstream of the catalyst. Nitrogen oxides, NH_3, and O_2 react on the surface of the catalyst to form N_2 and H_2O. For the SCR system to operate properly, the exhaust gas must be within a particular temperature range (typically between 450 and 850°F). The temperature range is dictated by the catalyst (typically made from noble metals, base metal oxides such as vanadium and titanium, and zeolite-based material). Exhaust gas temperatures greater than the upper limit (850°F) will pass the NO_x and ammonia unreacted through the catalyst. Ammonia emissions, called NH_3 slip, are a key consideration when specifying a SCR system. SCR is most suitable for lean-burn engines operated at constant loads, and can achieve efficiencies as high as 90 percent. For engines which typically operate at variable loads, such as engines on gas transmission pipelines, an SCR system may not function effectively, causing either periods of ammonia slip or insufficient ammonia to gain the reductions needed.

Catalytic Oxidation -

Catalytic oxidation is a postcombustion technology that has been applied, in limited cases, to oxidize CO in engine exhaust, typically from lean-burn engines. As previously mentioned, lean-burn technologies may cause increased CO emissions. The application of catalytic oxidation has been shown to be effective in reducing CO emissions from lean-burn engines. In a catalytic oxidation system, CO passes over a catalyst, usually a noble metal, which oxidizes the CO to CO_2 at efficiencies of approximately 70 percent for 2SLB engines and 90 percent for 4SLB engines.

3.2.5 Updates Since the Fifth Edition

The Fifth Edition was released in January 1995. Revisions to this section since that date are summarized below. For further detail, consult the memoranda describing each supplement or the background report for this section. These and other documents can be found on the Clearinghouse for Inventories/Emission Factors (CHIEF) electronic bulletin board (919-541-5742), or on the new Emission Factor and Inventory Group (EFIG) home page (http://www.epa.gov/ttn/chief).

Supplement A, February 1996

- In the table for uncontrolled natural gas prime movers, the Source Classification Code (SCC) for 4-cycle lean-burn was changed from 2-01-002-53 to 2-02-002-54. The SCC for 4-cycle rich-burn was changed from 2-02-002-54 to 2-02-02-002-53.

- An SCC (2-02-002-53) was provided for 4-cycle rich-burn engines, and the "less than" symbol (<) was restored to the appropriate factors.

Supplement B, October 1996

- The introduction section was revised.

- Text was added concerning process description of turbines.

- Text concerning emissions and controls was revised.
- References in various tables were editorially corrected.
- The inconsistency between a CO_2 factor in the table and an equation in the footnote was corrected.

Supplement F, July 2000

- Turbines used for natural gas compression were removed from this section and combined with utility turbines in Section 3.1. Section 3.2 now only contains information on natural gas-fired reciprocating engines.
- All emission factors were updated based on emissions data points taken from 70 emission reports containing over 400 source tests. Many new emission factors have been incorporated in this section for speciated organic compounds, including hazardous air pollutants.

TABLE 3.2-1 UNCONTROLLED EMISSION FACTORS FOR 2-STROKE LEAN-BURN ENGINES[a]
(SCC 2-02-002-52)

Pollutant	Emission Factor (lb/MMBtu)[b] (fuel input)	Emission Factor Rating
Criteria Pollutants and Greenhouse Gases		
NO_x[c] 90 - 105% Load	3.17 E+00	A
NO_x[c] <90% Load	1.94 E+00	A
CO[c] 90 - 105% Load	3.86 E-01	A
CO[c] <90% Load	3.53 E-01	A
CO_2[d]	1.10 E+02	A
SO_2[e]	5.88 E-04	A
TOC[f]	1.64 E+00	A
Methane[g]	1.45 E+00	C
VOC[h]	1.20 E-01	C
PM10 (filterable)[i]	3.84 E-02	C
PM2.5 (filterable)[i]	3.84 E-02	C
PM Condensable[j]	9.91 E-03	E
Trace Organic Compounds		
1,1,2,2-Tetrachloroethane[k]	6.63 E-05	C
1,1,2-Trichloroethane[k]	5.27 E-05	C
1,1-Dichloroethane	3.91 E-05	C
1,2,3-Trimethylbenzene	3.54 E-05	D
1,2,4-Trimethylbenzene	1.11 E-04	C
1,2-Dichloroethane	4.22 E-05	D
1,2-Dichloropropane	4.46 E-05	C
1,3,5-Trimethylbenzene	1.80 E-05	D
1,3-Butadiene[k]	8.20 E-04	D
1,3-Dichloropropene[k]	4.38 E-05	C
2,2,4-Trimethylpentane[k]	8.46 E-04	B
2-Methylnaphthalene[k]	2.14 E-05	C
Acenaphthene[k]	1.33 E-06	C

Table 3.2-1. UNCONTROLLED EMISSION FACTORS FOR 2-STROKE LEAN-BURN ENGINES

(Continued)

Pollutant	Emission Factor (lb/MMBtu)[b] (fuel input)	Emission Factor Rating
Acenaphthylene[k]	3.17 E-06	C
Acetaldehyde[k,l]	7.76 E-03	A
Acrolein[k,l]	7.78 E-03	A
Anthracene[k]	7.18 E-07	C
Benz(a)anthracene[k]	3.36 E-07	C
Benzene[k]	1.94 E-03	A
Benzo(a)pyrene[k]	5.68 E-09	D
Benzo(b)fluoranthene[k]	8.51 E-09	D
Benzo(e)pyrene[k]	2.34 E-08	D
Benzo(g,h,i)perylene[k]	2.48 E-08	D
Benzo(k)fluoranthene[k]	4.26 E-09	D
Biphenyl[k]	3.95 E-06	C
Butane	4.75 E-03	C
Butyr/Isobutyraldehyde	4.37 E-04	C
Carbon Tetrachloride[k]	6.07 E-05	C
Chlorobenzene[k]	4.44 E-05	C
Chloroform[k]	4.71 E-05	C
Chrysene[k]	6.72 E-07	C
Cyclohexane	3.08 E-04	C
Cyclopentane	9.47 E-05	C
Ethane	7.09 E-02	A
Ethylbenzene[k]	1.08 E-04	B
Ethylene Dibromide[k]	7.34 E-05	C
Fluoranthene[k]	3.61 E-07	C
Fluorene[k]	1.69 E-06	C
Formaldehyde[k,l]	5.52 E-02	A

Table 3.2-1. UNCONTROLLED EMISSION FACTORS FOR 2-STROKE LEAN-BURN ENGINES (Concluded)

Pollutant	Emission Factor (lb/MMBtu)[b] (fuel input)	Emission Factor Rating
Indeno(1,2,3-c,d)pyrene[k]	9.93 E-09	D
Isobutane	3.75 E-03	C
Methanol[k]	2.48 E-03	A
Methylcyclohexane	3.38 E-04	C
Methylene Chloride[k]	1.47 E-04	C
n-Hexane[k]	4.45 E-04	C
n-Nonane	3.08 E-05	C
n-Octane	7.44 E-05	C
n-Pentane	1.53 E-03	C
Naphthalene[k]	9.63 E-05	C
PAH[k]	1.34 E-04	D
Perylene[k]	4.97 E-09	D
Phenanthrene[k]	3.53 E-06	C
Phenol[k]	4.21 E-05	C
Propane	2.87 E-02	C
Pyrene[k]	5.84 E-07	C
Styrene[k]	5.48 E-05	A
Toluene[k]	9.63 E-04	A
Vinyl Chloride[k]	2.47 E-05	C
Xylene[k]	2.68 E-04	A

[a] Reference 7. Factors represent uncontrolled levels. For NO_x, CO, and PM10, "uncontrolled" means no combustion or add-on controls; however, the factor may include turbocharged units. For all other pollutants, "uncontrolled" means no oxidation control; the data set may include units with control techniques used for NOx control, such as PCC and SCR for lean burn engines, and PSC for rich burn engines. Factors are based on large population of engines. Factors are for engines at all loads, except as indicated. SCC = Source Classification Code. TOC = Total Organic Compounds. PM10 = Particulate Matter ≤ 10 microns (μm) aerodynamic diameter. A "<" sign in front of a factor means that the corresponding emission factor is based on one-half of the method detection limit.

[b] Emission factors were calculated in units of (lb/MMBtu) based on procedures in EPA

Method 19. To convert from (lb/MMBtu) to (lb/10^6 scf), multiply by the heat content of the fuel. If the heat content is not available, use 1020 Btu/scf. To convert from (lb/MMBtu) to (lb/hp-hr) use the following equation:

$$\text{lb/hp-hr} = (\text{lb/MMBtu})\ (\text{heat input, MMBtu/hr})\ (1/\text{operating HP, 1/hp})$$

[c] Emission tests with unreported load conditions were not included in the data set.

[d] Based on 99.5% conversion of the fuel carbon to CO_2. CO_2 [lb/MMBtu] = (3.67)(%CON)(C)(D)(1/h), where %CON = percent conversion of fuel carbon to CO_2, C = carbon content of fuel by weight (0.75), D = density of fuel, 4.1 E+04 lb/10^6 scf, and h = heating value of natural gas (assume 1020 Btu/scf at 60°F).

[e] Based on 100% conversion of fuel sulfur to SO_2. Assumes sulfur content in natural gas of 2,000 gr/10^6 scf.

[f] Emission factor for TOC is based on measured emission levels of 43 tests.

[g] Emission factor for methane is determined by subtracting the VOC and ethane emission factors from the TOC emission factor. Measured emission factor for methane compares well with the calculated emission factor, 1.48 lb/MMBtu vs. 1.45 lb/MMBtu, respectively.

[h] VOC emission factor is based on the sum of the emission factors for all speciated organic compounds less ethane and methane.

[i] Considered ≤ 1 μm in aerodynamic diameter. Therefore, for filterable PM emissions, PM10(filterable) = PM2.5(filterable).

[j] No data were available for condensable PM emissions. The presented emission factor reflects emissions from 4SLB engines.

[k] Hazardous Air Pollutant as defined by Section 112(b) of the Clean Air Act.

[l] For lean burn engines, aldehyde emissions quantification using CARB 430 may reflect interference with the sampling compounds due to the nitrogen concentration in the stack. The presented emission factor is based on FTIR measurements. Emissions data based on CARB 430 are available in the background report.

Table 3.2-2. UNCONTROLLED EMISSION FACTORS FOR 4-STROKE LEAN-BURN ENGINES[a]
(SCC 2-02-002-54)

Pollutant	Emission Factor (lb/MMBtu)[b] (fuel input)	Emission Factor Rating
Criteria Pollutants and Greenhouse Gases		
NO_x[c] 90 - 105% Load	4.08 E+00	B
NO_x[c] <90% Load	8.47 E-01	B
CO[c] 90 - 105% Load	3.17 E-01	C
CO[c] <90% Load	5.57 E-01	B
CO_2[d]	1.10 E+02	A
SO_2[e]	5.88 E-04	A
TOC[f]	1.47 E+00	A
Methane[g]	1.25 E+00	C
VOC[h]	1.18 E-01	C
PM10 (filterable)[i]	7.71 E-05	D
PM2.5 (filterable)[i]	7.71 E-05	D
PM Condensable[j]	9.91 E-03	D
Trace Organic Compounds		
1,1,2,2-Tetrachloroethane[k]	<4.00 E-05	E
1,1,2-Trichloroethane[k]	<3.18 E-05	E
1,1-Dichloroethane	<2.36 E-05	E
1,2,3-Trimethylbenzene	2.30 E-05	D
1,2,4-Trimethylbenzene	1.43 E-05	C
1,2-Dichloroethane	<2.36 E-05	E
1,2-Dichloropropane	<2.69 E-05	E
1,3,5-Trimethylbenzene	3.38 E-05	D
1,3-Butadiene[k]	2.67E-04	D
1,3-Dichloropropene[k]	<2.64 E-05	E
2-Methylnaphthalene[k]	3.32 E-05	C
2,2,4-Trimethylpentane[k]	2.50 E-04	C
Acenaphthene[k]	1.25 E-06	C

Table 3.2-2. UNCONTROLLED EMISSION FACTORS FOR 4-STROKE LEAN-BURN ENGINES
(Continued)

Pollutant	Emission Factor (lb/MMBtu)[b] (fuel input)	Emission Factor Rating
Acenaphthylene[k]	5.53 E-06	C
Acetaldehyde[k,l]	8.36 E-03	A
Acrolein[k,l]	5.14 E-03	A
Benzene[k]	4.40 E-04	A
Benzo(b)fluoranthene[k]	1.66 E-07	D
Benzo(e)pyrene[k]	4.15 E-07	D
Benzo(g,h,i)perylene[k]	4.14 E-07	D
Biphenyl[k]	2.12 E-04	D
Butane	5.41 E-04	D
Butyr/Isobutyraldehyde	1.01 E-04	C
Carbon Tetrachloride[k]	<3.67 E-05	E
Chlorobenzene[k]	<3.04 E-05	E
Chloroethane	1.87 E-06	D
Chloroform[k]	<2.85 E-05	E
Chrysene[k]	6.93 E-07	C
Cyclopentane	2.27 E-04	C
Ethane	1.05 E-01	C
Ethylbenzene[k]	3.97 E-05	B
Ethylene Dibromide[k]	<4.43 E-05	E
Fluoranthene[k]	1.11 E-06	C
Fluorene[k]	5.67 E-06	C
Formaldehyde[k,l]	5.28 E-02	A
Methanol[k]	2.50 E-03	B
Methylcyclohexane	1.23 E-03	C
Methylene Chloride[k]	2.00 E-05	C
n-Hexane[k]	1.11 E-03	C
n-Nonane	1.10 E-04	C

Table 3.2-2. UNCONTROLLED EMISSION FACTORS FOR 4-STROKE LEAN-BURN ENGINES
(Continued)

Pollutant	Emission Factor (lb/MMBtu)[b] (fuel input)	Emission Factor Rating
n-Octane	3.51 E-04	C
n-Pentane	2.60 E-03	C
Naphthalene[k]	7.44 E-05	C
PAH[k]	2.69 E-05	D
Phenanthrene[k]	1.04 E-05	D
Phenol[k]	2.40 E-05	D
Propane	4.19 E-02	C
Pyrene[k]	1.36 E-06	C
Styrene[k]	<2.36 E-05	E
Tetrachloroethane[k]	2.48 E-06	D
Toluene[k]	4.08 E-04	B
Vinyl Chloride[k]	1.49 E-05	C
Xylene[k]	1.84 E-04	B

[a] Reference 7. Factors represent uncontrolled levels. For NO_x, CO, and PM10, "uncontrolled" means no combustion or add-on controls; however, the factor may include turbocharged units. For all other pollutants, "uncontrolled" means no oxidation control; the data set may include units with control techniques used for NOx control, such as PCC and SCR for lean burn engines, and PSC for rich burn engines. Factors are based on large population of engines. Factors are for engines at all loads, except as indicated. SCC = Source Classification Code. TOC = Total Organic Compounds. PM-10 = Particulate Matter ≤ 10 microns (μm) aerodynamic diameter. A "<" sign in front of a factor means that the corresponding emission factor is based on one-half of the method detection limit.

[b] Emission factors were calculated in units of (lb/MMBtu) based on procedures in EPA Method 19. To convert from (lb/MMBtu) to (lb/10^6 scf), multiply by the heat content of the fuel. If the heat content is not available, use 1020 Btu/scf. To convert from (lb/MMBtu) to (lb/hp-hr) use the following equation:

$$\text{lb/hp-hr} = (\text{lb/MMBtu})\ (\text{heat input, MMBtu/hr})\ (1/\text{operating HP, 1/hp})$$

[c] Emission tests with unreported load conditions were not included in the data set.

[d] Based on 99.5% conversion of the fuel carbon to CO_2. CO_2 [lb/MMBtu] = (3.67)(%CON)(C)(D)(1/h), where %CON = percent conversion of fuel carbon to CO_2, C = carbon content of fuel by weight (0.75), D = density of fuel, 4.1 E+04 lb/10^6 scf, and

h = heating value of natural gas (assume 1020 Btu/scf at 60°F).

[e] Based on 100% conversion of fuel sulfur to SO_2. Assumes sulfur content in natural gas of 2,000 gr/10^6 scf.

[f] Emission factor for TOC is based on measured emission levels from 22 source tests.

[g] Emission factor for methane is determined by subtracting the VOC and ethane emission factors from the TOC emission factor. Measured emission factor for methane compares well with the calculated emission factor, 1.31 lb/MMBtu vs. 1.25 lb/MMBtu, respectively.

[h] VOC emission factor is based on the sum of the emission factors for all speciated organic compounds less ethane and methane.

[i] Considered ≤ 1 μm in aerodynamic diameter. Therefore, for filterable PM emissions, PM10(filterable) = PM2.5(filterable).

[j] PM Condensable = PM Condensable Inorganic + PM-Condensable Organic

[k] Hazardous Air Pollutant as defined by Section 112(b) of the Clean Air Act.

[l] For lean burn engines, aldehyde emissions quantification using CARB 430 may reflect interference with the sampling compounds due to the nitrogen concentration in the stack. The presented emission factor is based on FTIR measurements. Emissions data based on CARB 430 are available in the background report.

Table 3.2-3. UNCONTROLLED EMISSION FACTORS FOR 4-STROKE RICH-BURN ENGINES[a]
(SCC 2-02-002-53)

Pollutant	Emission Factor (lb/MMBtu)[b] (fuel input)	Emission Factor Rating
Criteria Pollutants and Greenhouse Gases		
NO_x[c] 90 - 105% Load	2.21 E+00	A
NO_x[c] <90% Load	2.27 E+00	C
CO[c] 90 - 105% Load	3.72 E+00	A
CO[c] <90% Load	3.51 E+00	C
CO_2[d]	1.10 E+02	A
SO_2[e]	5.88 E-04	A
TOC[f]	3.58 E-01	C
Methane[g]	2.30 E-01	C
VOC[h]	2.96 E-02	C
PM10 (filterable)[i,j]	9.50 E-03	E
PM2.5 (filterable)[j]	9.50 E-03	E
PM Condensable[k]	9.91 E-03	E
Trace Organic Compounds		
1,1,2,2-Tetrachloroethane[l]	2.53 E-05	C
1,1,2-Trichloroethane[l]	<1.53 E-05	E
1,1-Dichloroethane	<1.13 E-05	E
1,2-Dichloroethane	<1.13 E-05	E
1,2-Dichloropropane	<1.30 E-05	E
1,3-Butadiene[l]	6.63 E-04	D
1,3-Dichloropropene[l]	<1.27 E-05	E
Acetaldehyde[l,m]	2.79 E-03	C
Acrolein[l,m]	2.63 E-03	C
Benzene[l]	1.58 E-03	B
Butyr/isobutyraldehyde	4.86 E-05	D
Carbon Tetrachloride[l]	<1.77 E-05	E

Table 3.2-3. UNCONTROLLED EMISSION FACTORS FOR 4-STROKE RICH-BURN ENGINES (Concluded)

Pollutant	Emission Factor (lb/MMBtu)[b] (fuel input)	Emission Factor Rating
Chlorobenzene[l]	<1.29 E-05	E
Chloroform[l]	<1.37 E-05	E
Ethane[n]	7.04 E-02	C
Ethylbenzene[l]	<2.48 E-05	E
Ethylene Dibromide[l]	<2.13 E-05	E
Formaldehyde[l,m]	2.05 E-02	A
Methanol[l]	3.06 E-03	D
Methylene Chloride[l]	4.12 E-05	C
Naphthalene[l]	<9.71 E-05	E
PAH[l]	1.41 E-04	D
Styrene[l]	<1.19 E-05	E
Toluene[l]	5.58 E-04	A
Vinyl Chloride[l]	<7.18 E-06	E
Xylene[l]	1.95 E-04	A

[a] Reference 7. Factors represent uncontrolled levels. For NO_x, CO, and PM-10, "uncontrolled" means no combustion or add-on controls; however, the factor may include turbocharged units. For all other pollutants, "uncontrolled" means no oxidation control; the data set may include units with control techniques used for NOx control, such as PCC and SCR for lean burn engines, and PSC for rich burn engines. Factors are based on large population of engines. Factors are for engines at all loads, except as indicated. SCC = Source Classification Code. TOC = Total Organic Compounds. PM10 = Particulate Matter ≤ 10 microns (μm) aerodynamic diameter. A "<" sign in front of a factor means that the corresponding emission factor is based on one-half of the method detection limit.

[b] Emission factors were calculated in units of (lb/MMBtu) based on procedures in EPA Method 19. To convert from (lb/MMBtu) to (lb/10^6 scf), multiply by the heat content of the fuel. If the heat content is not available, use 1020 Btu/scf. To convert from (lb/MMBtu) to (lb/hp-hr) use the following equation:

$$\text{lb/hp-hr} = (\text{lb/MMBtu})\,(\text{heat input, MMBtu/hr})\,(1/\text{operating HP, 1/hp})$$

[c] Emission tests with unreported load conditions were not included in the data set.

[d] Based on 99.5% conversion of the fuel carbon to CO_2. CO_2 [lb/MMBtu] = (3.67)(%CON)(C)(D)(1/h), where %CON = percent conversion of fuel carbon to CO_2,

C = carbon content of fuel by weight (0.75), D = density of fuel, 4.1 E+04 lb/10^6 scf, and h = heating value of natural gas (assume 1020 Btu/scf at 60°F).

[e] Based on 100% conversion of fuel sulfur to SO_2. Assumes sulfur content in natural gas of 2,000 gr/10^6scf.

[f] Emission factor for TOC is based on measured emission levels from 6 source tests.

[g] Emission factor for methane is determined by subtracting the VOC and ethane emission factors from the TOC emission factor.

[h] VOC emission factor is based on the sum of the emission factors for all speciated organic compounds. Methane and ethane emissions were not measured for this engine category.

[i] No data were available for uncontrolled engines. PM10 emissions are for engines equipped with a PCC.

[j] Considered ≤ 1 μm in aerodynamic diameter. Therefore, for filterable PM emissions, PM10(filterable) = PM2.5(filterable).

[k] No data were available for condensable emissions. The presented emission factor reflects emissions from 4SLB engines.

[l] Hazardous Air Pollutant as defined by Section 112(b) of the Clean Air Act.

[m] For rich-burn engines, no interference is suspected in quantifying aldehyde emissions. The presented emission factors are based on FTIR and CARB 430 emissions data measurements.

[n] Ethane emission factor is determined by subtracting the VOC emission factor from the NMHC emission factor.

References For Section 3.2

1. *Engines, Turbines, And Compressors Directory*, American Gas Association, Catalog #XF0488.

2. *Standards Support And Environmental Impact Statement, Volume I: Stationary Internal Combustion Engines*, EPA-450/2-78-125a, U. S. Environmental Protection Agency, Office of Air Quality Planning and Standards, Research Triangle Park, NC, July 1979.

3. *Alternative Control Techniques Document - NO_x Emissions From Stationary Reciprocating Engines*, EPA-453/R-93-032, July 1993.

4. *Handbook - Control Technologies For Hazardous Air Pollutants*, EPA-625/6-91-014, June 1991.

5. *Limiting Net Greenhouse Gas Emissions In The United States, Volume II: Energy Responses,* Report for the Office of Environmental Analysis, Office of Policy, Planning and Analysis, Department of Energy (DOE), DOE/PE-0101 Volume II, September 1991.

6. C. Castaldini, *NO_x Reduction Technologies For Natural Gas Industry Prime Movers*, GRI-90/0215, Gas Research Institute, Chicago, IL, August 1990.

7. *Emission Factor Documentation for AP-42 Section 3.2, Natural Gas-Fired Reciprocating Engines*, EPA Contract No. 68-D2-0160, Alpha-Gamma Technologies, Inc., Raleigh, North Carolina, July 2000.

to be reduced to ensure that we stay in or below the lower warming range?
If the industrialized world were to follow California's lead of reducing emissions 80 percent below 1990 levels by 2050 and the industrializing nations followed thereafter, global emissions would remain in or below the lower emissions scenario, thus increasing the likelihood that California and the world would be on track to avoid the more severe impacts.

California's Responsibility to Act
California is the 12th largest source of global warming emissions in the world, exceeding most entire countries. California has a responsibility to reduce its global warming emissions, and by doing so can lead the United States, and the world, in developing the innovative policies and technologies needed to avoid the most dangerous impacts of global warming. Two independent teams of the state's top economists calculate that significantly reducing global warming emissions can boost the state's economy by billions of dollars and create tens of thousands of jobs in the coming decades.

Global Warming Emission Reduction Targets
In June 2005 Governor Schwarzenegger signed an Executive Order committing the state to the following targets for reducing global warming emissions:

- By 2010, California emissions will be reduced to 2000 levels, or by 11 percent
- By 2020, California emissions will be reduced to 1990 levels, or by 25 percent
- By 2050, California emissions will be reduced to 80 percent below 1990 levels

Policy Recommendations for 2006
A strong, enforceable cap on global warming emissions will be needed to achieve the reductions called for in the governor's targets. The governor and legislature should work together to codify the governor's targets and create an enforceable and declining cap on global warming emissions for the sectors of the economy that comprise the largest

emitters. In order for a cap to work, verifiable mandatory reporting of global warming emissions for those sectors will be required.

Sector-specific regulatory programs offer important opportunities for reducing emissions as well. Implementing aggressive renewable energy and energy efficiency policies for all electric providers in the state is essential. As the transportation sector will continue to be the largest source of global warming emissions in California for the foreseeable future, additional measures will be needed beyond the landmark emissions standards for vehicles now in place. For example, a self-financing program of emission-based discounts and surcharges on new cars will help consumers and families purchase cleaner new cars and encourage auto manufacturers to offer cleaner, more efficient cars to California drivers.

Page Last Revised: 03/02/06